Supersymmetric electroweak radiative corrections to $e^+e^- \longrightarrow W^+W^-$. I

S. Alam*
Ottawa Carleton Institute for Physics, Carleton University, Ottawa, Canada
(Received 18 November 1991; revised manuscript received 4 October 1993)

This is the first of a series of three papers in which we give a complete analysis of one loop quantum corrections to the W pair production in the context of supersymmetric electroweak theory. We have adopted the on-mass-shell subtraction scheme of Sakakibara and previously demonstrated the consistency of this scheme. The relevant analytic results are given, and the one-loop-corrected differential cross section incorporating the finite corrections is written out. A complete computer program for the calculations of these corrections has been developed. This program has been checked in several ways to ensure against errors in this long calculation where many subtle cancellations are involved. In this paper we give an outline of our model, sketch our renormalization procedure, and give analytic and numerical results for the self-energy insertions, wave function renormalization, and soft-photon bremsstrahlung. We find that the percentage (with respect to the tree-level) of *virtual* loop corrections (considered in this paper) due to the addition of SUSY particles varies approximately from -5.93% to -5.21%. As a comparison the percentage *virtual* corrections due to self-energy insertions and wave function renormalization in the SM varies typically from 27.9% to 20.3%. The SM total percentage *virtual* loop corrections varies typically from 17.4% to 19%. The above comparison is made at the same center-of-mass energy (200 GeV). The first percentage in this comparison is for center-of-mass angles of 10°, the second being at 90°.

PACS number(s): 13.10.+q, 11.30.Pb, 12.60.Jv

I. INTRODUCTION

Supersymmetry is one of the most elegant extensions of the standard model. It solves the hierarchy problem, one of the major drawbacks of grand unified theories, by introducing a fermion-boson symmetry. It is precisely this beautiful property of supersymmetry which provides a hope of unifying all forces of nature,[1] and also allows forces and matter to be treated on the same footing. As a consequence of the Fermi-Bose symmetry, many new degrees of freedom corresponding to the supersymmetric partners (SP's) of the ordinary particles are predicted by the theory. However aesthetically appealing a theory might be, it must stand the test of experiment. Therefore it is of crucial interest to explore all the phenomenological implications of supersymmetric theories in order to eventually confront experiment.

A lot of work has been done on supersymmetric phenomenology [1–4]. The effect of supersymmetry on the physical properties (such as $g-2$ of leptons [5], the two-photon decay widths [6], the magnetic and the quadrupole [7] moments of the W boson) has received some attention. Radiative corrections in $N=1$ supersymmetry have been given in the context of neutral current scattering $e\nu_\mu \longrightarrow e\nu_\mu$, by Grifols [8] *et al.* and Schwarzer [9] and for $e^+e^- \longrightarrow \mu^+\mu^-$ by Lynn [10]. In Ref. [8] no mention is made of the renormalization scheme adopted. Schwarzer [9] adopts the minimal subtraction (MS) scheme and finds the electroweak parameters dependence on the supersymmetric effects to be small; for example, a 0.002 increase is found in the value of $\sin^2\theta_W(\mu^2)$ at scale $\mu^2 = M_W^2$ and a small decrease of the order of few MeV in the predicted gauge boson masses. A good review of phenomenology and work on the radiative corrections both in and beyond the standard model may be found in [1].

The purpose of this paper (and two others) is to report on our [11] calculation of the one loop radiative corrections to the process $e^+e^- \longrightarrow W^+W^-$ in the supersymmetric Weinberg-Salam (WS) [or quantum flavor dynamics (QFD)] model. Radiative corrections to $e^+e^- \longrightarrow W^+W^-$ in QFD were first calculated by Lemoine and Veltman [12] and Philippe [13]. More recently they were repeated by Bohm *et al.* [14], Fleischer [15] and us.[2] The importance of the reaction $e^+e^- \longrightarrow W^+W^-$ as a test of the standard model cannot be overemphasized. Despite the recent results at CERN e^+e^- collider LEP I pointing to the success of the standard model, the Higgs boson and the top quark have eluded detection. Moreover the crucial feature of the WS model, i.e., a test of the triple boson vertices still has to be made. One place where the triple boson vertices will be tested is in the electron positron annihilation into pairs of charged vector bosons at LEP II. Another quantity to be measured (with great precision) at LEP II is of course the W-boson mass, expected to be measured within an accuracy of 100 MeV. This coupled with the now well-determined Z-boson mass

*Now at the Department of Physics, University of Peshawar, Peshawar, NWFP, Pakistan.

[1]We mean generalizations of global supersymmetry like supergravity and superstring theories.

[2]By "us" we mean M.K. Sundaresan, P. Kalyniak, and the author.

[16] will make it possible to detect deviations from the standard model. This necessitates all the more that the standard model radiative corrections (at least up to one loop) be accurately estimated. Thus, many independent evaluations are necessary, which will allow the experimentalists to compare their results with the theoretical predictions with some confidence. It would also be interesting to estimate the change in the one-loop-corrected differential cross section that would arise as a result of the addition of supersymmetric (SUSY) particles. In particular one may ask the question how sensitive is the differential cross section to the process $e^+e^- \longrightarrow W^+W^-$ to the SP masses. In order to answer the latter question we took the SP masses near their present experimental limits and we also considered the case when most of the SP masses are greater than the W mass.

The arrangement of this paper is as follows. A brief description of our model is given in Sec. II . Section III contains a discussion of the lowest-order differential cross section. In Sec. IV we briefly review our renormalization scheme and give a brief description of the structure of the virtual corrections and of the systematic evaluation of the one-loop Feynman diagrams. Section V contains the analytic and numerical results of all the self-energy corrections. A complete discussion of the bremsstrahlung cross section is contained in Sec. VI. Finally the Appendices contains the necessary collection of the formulas for the virtual corrections.

II. THE MODEL

When studying the phenomenology of various processes involving supersymmetric particles, it is convenient to choose some model. However it is desirable to proceed in as much as possible in a model-independent way. With this in mind we have chosen to work with a softly broken supersymmetric extension of QFD (SQFD) of Haber and Kane [2]. The complete Lagrangian is given in [11] and will not be repeated here, but we briefly recall the particle content of this model [2]. It consists of the following five physical multiplets $(\gamma,\tilde{\gamma})$, $(W^-,\tilde{\omega}_1^-,H^-)$, $(W^+,\tilde{\omega}_2^+,H^+)$, $(Z,\tilde{z},H_2^0)$, and $(H_1^0,H_3^0,\sqrt{2}\mathrm{ReN},\sqrt{2}\mathrm{ImN},\tilde{h})$. In the supersymmetric (SUSY) limit these have masses 0, M_W, M_W, M_Z, and $m_{H_1^0}$ respectively. We note that here H_1^0 is the physical Higgs particle of QFD. The above multiplets consist of an equal number of Bose and Fermi degrees of freedom. In the above multiplets $\tilde{\omega}_1^-$, $\tilde{\omega}_2^+$, $\tilde{z}$, $\tilde{h}$, are given by

$$\tilde{\omega}_1^- = \begin{bmatrix} \psi^2_{H_1} \\ i\bar{\lambda}^+ \end{bmatrix},$$

$$\tilde{\omega}_2^+ = \begin{bmatrix} \psi^1_{H_2} \\ i\bar{\lambda}^- \end{bmatrix},$$

$$\tilde{z} = \begin{bmatrix} \frac{\psi^1_{H_1}-\psi^2_{H_2}}{\sqrt{2}} \\ i\bar{\lambda}_z \end{bmatrix},$$

and

$$\tilde{h} = \begin{bmatrix} \frac{\psi^1_{H_1}+\psi^2_{H_2}}{\sqrt{2}} \\ i\bar{\psi}_N \end{bmatrix}.$$

The various Higgs fields are extracted from

$$H_1 = \begin{bmatrix} \frac{1}{2}[H_1^0 - H_2^0 + i(H_3^0 - G^0)] \\ \frac{1}{\sqrt{2}}[H^- - G^-] \end{bmatrix},$$

and

$$H_2 = \begin{bmatrix} \frac{1}{\sqrt{2}}[H^+ + G^+] \\ \frac{1}{2}[H_1^0 + H_2^0 + i(H_3^0 + G^0)] \end{bmatrix}.$$

For example H^+ is defined as

$$H^+ = \frac{1}{\sqrt{2}}(H_2^1 + H_1^{2*}).$$

In all our calculations we have used the above physical component fields. We stress that we have not used the superfield formalism for the loop calculations.

Our conventions are those of Bjorken and Drell [17]. The various notations adopted here are as follows.

(1) The metric convention $(+,-,-,-)$ is chosen.

(2) The Wess-Zumino gauge is chosen for the vector superfield (it is well known [18] that this leaves the Faddeev-Popov ghost sector unchanged).

(3) Dimensional regularization is used with

$$\triangle = -\frac{2}{\varepsilon} - \gamma_E + \ln(4\pi\mu^2) - \ln(M_W^2) + O(\varepsilon),$$

$$n = 4 + \varepsilon.$$

In using dimensional regularization in conjunction with on-mass-shell renormalization scheme we [11] (see e.g., work by P. Kalyniak and M.K. Sundaresan cited in [11]) have used $g_\mu^\mu = n$, $\mathrm{Tr}\, I = n$ consistently. Using n instead of 4 leads to extra finite constant terms.

(4) We work in the 't Hooft–Feynman gauge.

The following abbreviations have been used: $s_W = \sin\theta_W$, $c_W = \cos\theta_W$, $t_W = \tan\theta_W$, f denotes fermion, $\tilde{f}$ is a shorthand for the sfermion, GB stands for vector boson and $\doteq$ is equivalent to $= \frac{g^2}{16\pi^2}$. We also use uppercase to denote particles, F stands for fermion, B for boson, SF and SB denote respectively the corresponding supersymmetric partners of F and B. SP stands for supersymmetric partners of the ordinary particles. fct is a shorthand for finite parts of the counterterms. The subscript 1 has been used to remind ourselves that we are working to the first order in the coupling constant. QFD and SQFD are acronyms for quantum flavor dynamics and supersymmetric quantum flavor dynamics respectively.

In this paper, for the purposes of numerical evaluations, we assume the following values for our set of independent input parameters [16]: $\alpha = 1/137.035985$ and the listing of input masses in GeV given in Table I.

TABLE I. Listing of input masses in GeV.

Particles	Mass	SUSY Particles	Mass
m_e	0.000511	$m_{\tilde{e}}$	45.0
m_{ν_e}	0	$m_{\tilde{\nu_e}}$	30.0
m_μ	0.105658	$m_{\tilde{\mu}}$	45.1057
m_{ν_μ}	0	$m_{\tilde{\nu_\mu}}$	30.0
m_τ	1.7841	$m_{\tilde{\tau}}$	46.7841
m_{ν_τ}	0	$m_{\tilde{\nu_\tau}}$	30.0
m_u	0.032	$m_{\tilde{u}}$	45.032
m_d	0.032	$m_{\tilde{d}}$	45.032
m_c	1.5	$m_{\tilde{c}}$	46.5
m_s	0.15	$m_{\tilde{s}}$	45.15
m_t	100.0	$m_{\tilde{t}}$	50.0
m_b	4.5	$m_{\tilde{b}}$	49.5
$m_{H_1^0}$	50, 100.0	$m_{H_3^0}$	75.0
M_W	81.0, 82.0	m_{H^+}	91.0
M_Z	92.0, 93.0	$m_{H_2^0}$	100.0
SP	Mass	SP	Mass
$m_{\tilde{\gamma}}$	15.0	$m_{\tilde{\omega}}$	50.0
$m_{\tilde{z}}$	35.0	$m_{\tilde{h}}$	40.0

The following remarks are in order as to why we have chosen this particular set of the input parameters.

(1) It is necessary to make a sensible comparison with the results given by other authors [12–15]. For the purposes of exact comparison [19,20] with the work of [14] we take $M_W = 82.0$, $M_Z = 93.0$, and $m_{H_1^0} = 100.0$.

(2) The input masses for the supersymmetric particles given above were inspired by the work of Baer *et al.* [21], and by the experimental limits [16]. The masses given above for the supersymmetric Higgs sector were arrived at by keeping in mind the recent experimental limits [16] and the standard wisdom (that at the tree-level) $m_{H^+} > M_W$, $m_{H_2^0} > M_Z$, $m_{H_3^0} > m_{H_1^0}$, and $m_{H_1^0} < M_Z$. In addition to the case given above for the SUSY particles masses we [20] also examine the case where the masses of most SUSY particles are taken above the W-boson mass. However we have kept the photino mass light in both of the cases we [20] have considered.

III. BORN CROSS SECTION

The tree-level cross section for the process $e^+e^- \longrightarrow W^+W^-$ in QFD has been extensively quoted in literature since its first calculation by Alles *et al.* [22]. Here we establish notation, give definitions, and briefly discuss the unpolarized differential cross section for this process. It is known that to get more realistic results the decay of W's into fermion pairs must be considered. We present the polarization summed squared amplitudes for off-shell W's so that it will be useful as a part of a more complete radiative correction program for four fermion production processes. In the limit that the W's are on-shell our expression reduces to the well-known result [22,12,13]. A number of misprints in [12] have been pointed out by Philippe [13]. The effects of polarized electron positron beams are discussed by [15].

The momenta of the incoming positron and electron and the outgoing W^+ and W^- are denoted respectively by p_1, p_2, q_1, and q_2. The invariants of the process are given by (when the W's are off shell)

$$p_1^2 = m_e^2, \tag{1}$$
$$p_2^2 = m_e^2, \tag{2}$$
$$q_1^2 = s_3, \tag{3}$$
$$q_2^2 = s_4, \tag{4}$$

for the on-mass W's, $s_3 = s_4 = M_W^2$. The Mandelstam variables are defined in the usual manner:

$$s = [p_1 + p_2]^2 = [q_1 + q_2]^2, \tag{5}$$
$$t = [q_1 - p_1]^2 = [p_2 - q_2]^2, \tag{6}$$
$$u = [q_2 - p_1]^2 = [p_2 - q_1]^2, \tag{7}$$
$$s + t + u = 2m_e^2 + s_3 + s_4. \tag{8}$$

In terms of the center of mass (c.m.) scattering angle[3] θ, the beam energy E_b, and the c.m. energy $E_{\text{c.m.}}$, the above expressions [(5) through (8)] may be rewritten as

$$s = E_{\text{c.m.}}^2 = 4E_b^2, \tag{9}$$
$$t = m_e^2 + s_4 - \frac{s}{2}\left(1 + \frac{s_4 - s_3}{s} - \beta_e \frac{2q^\star}{\sqrt{s}} \cos\theta\right), \tag{10}$$
$$u = s_3 + s_4 + 2m_e^2 - s - t, \tag{11}$$

where

$$\beta_i = \sqrt{1 - \frac{4p_i^2}{s}} \tag{12}$$

is the velocity of the ith particle, and p_i is its four-momenta. $q^\star$ is the c.m. momentum of the W.

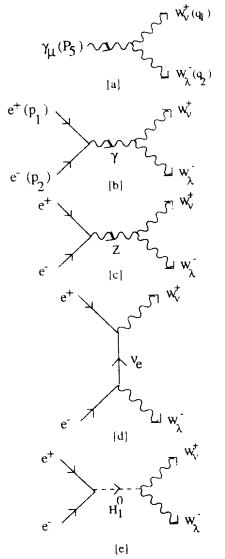

FIG. 1. The lowest order Feynman diagrams for the process $e^+e^- \longrightarrow W^+W^-$ and the three vertex momentum convention.

[3]Where we take θ to be the angle between the electron and the W^- direction.

The contributions to the lowest order Born cross section come from the three diagrams of Figs. 1(b)–1(d). Since the Higgs exchange contributes m_e^2/M_W^2 relative to the remaining three it can be neglected. The contribution to lowest-order amplitude can be succinctly written as

$$\mathcal{M}_0 = ig^2[\bar{v}(p_1)\gamma^\mu(a_s + b_s\gamma_5)u(p_2)\Gamma_{\mu\nu\lambda}\epsilon_1^\nu\epsilon_2^\lambda] \\ -ig^2[\bar{v}(p_1)\not{\epsilon}_1(\not{q}_1 - \not{p}_1)\not{\epsilon}_2(a_t + b_t\gamma_5)u(p_2)]. \quad (13)$$

Here

$$a_s = \frac{s_W^2}{s} + \frac{[1-4s_W^2]}{4[s-M_Z^2]}, \quad (14)$$

$$b_s = \frac{-1}{4[s-M_Z^2]}, \quad (15)$$

$$a_t = \frac{1}{4t}, \quad (16)$$

$$b_t = -a_t, \quad (17)$$

and

$$\Gamma_{\mu\nu\lambda} = g_{\mu\lambda}(p_5+q_2)_\nu + g_{\nu\lambda}(q_1-q_2)_\mu + g_{\mu\nu}(-p_5-q_1)_\lambda. \quad (18)$$

In Eq. (13) we have grouped the s-channel contributions from the photon (γ) and the Z boson into one term. By using the amplitude in Eq. (13), the polarization summed square amplitude is given by

$$\mathcal{A}_0(s,t,s_3,s_4) = (a_s^2+b_s^2)\mathcal{A}_{ss} + (a_t^2+b_t^2)\mathcal{A}_{tt} \\ -2(a_s\,a_t + b_s\,b_t)\mathcal{A}_{st}. \quad (19)$$

$\mathcal{A}_{ss}$ through $\mathcal{A}_{st}$ are given by

$$\mathcal{A}_{ss} = \frac{1}{s_3s_4}(q_1\cdot q_2)^2(2p_1\cdot p_2q_1\cdot q_2 - 2p_1\cdot q_1p_2\cdot q_2 - 2p_2\cdot q_1p_1\cdot q_2 + 2p_1\cdot q_1p_2\cdot q_1 \\ +2p_2\cdot q_2p_1\cdot q_2) + \frac{1}{s_4}q_1\cdot q_2(3q_1\cdot q_2p_1\cdot p_2 + 8p_1\cdot q_2p_2\cdot q_2 + 4p_1\cdot q_2p_2\cdot q_1 + 4p_1\cdot q_1p_2\cdot q_2) \\ +\frac{1}{s_3}q_1\cdot q_2(3q_1\cdot q_2p_1\cdot p_2 + 8p_1\cdot q_1p_2\cdot q_1 + 4p_1\cdot q_2p_2\cdot q_1 + 4p_1\cdot q_1p_2\cdot q_2) + 4p_1\cdot p_2q_1\cdot q_2 - 4p_1\cdot q_2p_2\cdot q_2 \\ -12p_1\cdot q_2p_2\cdot q_1 - 12p_1\cdot q_1p_2\cdot q_2 - 6s_3p_1\cdot p_2 - 4p_1\cdot q_1p_2\cdot q_1 - 6s_4p_1\cdot p_2, \quad (20)$$

$$\mathcal{A}_{st} = \frac{2}{s_3s_4}(q_1\cdot q_2)(p_2\cdot q_2)(-p_1\cdot p_2q_1\cdot q_2 \\ -2p_1\cdot q_1p_2\cdot q_1 + p_1\cdot q_2p_2\cdot q_1 + p_2\cdot q_2p_1\cdot q_1) + \frac{1}{s_4}p_2\cdot q_2[-4q_1\cdot q_2p_1\cdot p_2 \\ -2p_2\cdot q_2(p_1\cdot q_1 + 2p_1\cdot q_2) - 2p_2\cdot q_1p_1\cdot q_2] + \frac{1}{s_3}[2p_2\cdot q_1(p_2\cdot q_1[2p_1\cdot q_1 \\ +p_1\cdot q_2] + p_1\cdot q_1p_2\cdot q_2) + q_1\cdot q_2(p_1\cdot q_2p_2\cdot q_1 - 2p_1\cdot q_1p_2\cdot q_1 - 7p_2\cdot q_2p_1\cdot q_1 \\ -p_1\cdot p_2q_1\cdot q_2 - 2p_1\cdot p_2p_2\cdot q_1)] - 3p_1\cdot p_2q_1\cdot q_2 + 8p_1\cdot q_1p_2\cdot q_2 + 4s_4p_1\cdot p_2 \\ +2p_1\cdot p_2p_2\cdot q_2 + 6p_1\cdot p_2p_2\cdot q_1, \quad (21)$$

$$\mathcal{A}_{tt} = \left[-s_4 - 4p_2\cdot q_2 + \frac{4}{s_4}(p_2\cdot q_2)^2\right]\left(p_1\cdot p_2 + \frac{2}{s_3}p_1\cdot q_1p_2\cdot q_1\right) + 4(p_2\cdot q_2)\left[p_1\cdot q_2 + \frac{2}{s_3}p_1\cdot q_1q_1\cdot q_2s\right]. \quad (22)$$

The above analytic expression will be useful as an essential part of the tree-level cross section for the four fermion production process. For the on-shell W's (note from now on we take, for all numerical results, the W's to be on shell) the tree-level differential cross section is expressed as

$$\left(\frac{d\sigma(s,t,M_W^2,M_W^2)}{d\cos\theta}\right)_0 = \Phi\mathcal{A}_0(s,t,M_W^2,M_W^2), \quad (23)$$

where

$$\Phi = \frac{4g^4\beta_W\beta_e}{32\pi s}. \quad (24)$$

Numerical results are given in Tables II and III for the tree-level differential cross section. The values in Table II are in agreement with Philippe [13], taking into account that he uses different values for the masses of the W and Z bosons. Also he defines the center-of-mass angle as the angle between the direction of the electron and the W^+. In Table III we compare the effect of using two different schemes on the tree-level differential cross section. For a definition of the two schemes see the beginning of the next section. The change[4] $\delta\sigma$ of approximately 11

[4]The definition of $\delta\sigma$ is as follows:

$$\delta\sigma = \frac{\left(\frac{d\sigma}{d\cos\theta}\right)_0(\alpha) - \left(\frac{d\sigma}{d\cos\theta}\right)_0(G_\mu)}{\left(\frac{d\sigma}{d\cos\theta}\right)_0(G_\mu)}.$$

TABLE II. Standard model differential cross section in pb.

θ (deg)	$\left(\frac{d\sigma}{d\cos\theta}\right)_0$ (200GeV)	$\left(\frac{d\sigma}{d\cos\theta}\right)_0$ (500GeV)	$\left(\frac{d\sigma}{d\cos\theta}\right)_0$ (1000GeV)
10	155.6123	291.2080	83.0610
30	106.9359	33.1306	8.0082
50	59.3622	9.4963	2.2021
70	33.5360	3.7453	0.8379
90	20.5578	1.9066	0.4209
110	13.7370	1.1660	0.2582
130	9.8762	0.7161	0.1542
150	7.6402	0.3712	0.0684
170	6.5744	0.1665	0.0157

percent is quite substantial. This difference drops down significantly, as expected, after the inclusion of the one loop corrections. However there remains a non-negligible difference which signals higher order effects.

It should be pointed out that we have not averaged over the initial polarization states, to do so one simply divides by a factor of 4. We note that except for Table III for the purposes of all the analytic and numerical work given in this and the remaining two papers [19,20] we have used the alpha scheme.

IV. RENORMALIZATION SCHEME AND GENERAL STRUCTURE OF QUANTUM CORRECTIONS

In the on-mass subtraction procedure of Sakakibara [23] [on-mass-shell renormalization scheme (OMSRS)] the set of independent parameters in the alpha scheme is

$$(\alpha,\ M_W,\ M_Z,\ m_{H_1^0},\ m_f,\ m_s)$$

and, in the G_μ scheme,

$$(G_\mu,\ M_W,\ M_Z,\ m_{H_1^0},\ m_f,\ m_s),$$

where M_W is the W mass, M_Z is the Z mass, $m_{H_1^0}$ is the Higgs boson mass. m_f and m_s represent collectively the masses of the fermions and the supersymmetric particles respectively. Clearly the masses of the supersymmetric particles do not enter as independent input parameters in the SUSY limit [11]. The renormalization conditions are (1) the charge e is defined in the Thomson limit, and (2) all one particles irreducible two-point functions (including the vanishing of γZ mixing at $q^2 = 0$) have zeros at their physical masses. The ingredients needed to generate the counter terms in OMSRS of Sakakibara [23] are δg, $\delta g'$, δM_W, δM_Z, δZ_A, δZ_W, δZ_Z, δZ_L, and δZ_R. Of these δM_W, δM_Z, δZ_A, δZ_W, and δZ_Z are obtained from vector boson self-energies [23,11]. Sakakibara [23] considered explicitly the cancellation of divergences in the lepton–lepton–gauge-boson vertices. For his problem of radiative corrections to neutral current interactions, he was not concerned with the cancellation of the divergences in the three gauge boson vertices. This is, of course, what we need to do in our problem. We have demonstrated the cancellation of infinities within our model thus exhibiting the consistency of the adopted renormalization scheme [11]. Moreover we have shown the cancellation of the quadratic and linear divergences for all cases that occur in our model [11]. This is not merely an academic exercise since with so many diagrams to calculate one needs to check the calculation in every possible way.

Here we give the finite corrections and outline the OMSRS scheme along the way. Let us begin with the gauge boson sector. δM_W and δM_Z are obtained by the observation [23,11] that, by requiring the ghosts $(c^\pm, c_Z)$ self-energies to vanish at $q^2 = M_W^2$ and $q^2 = M_Z^2$ for $c^\pm$ and c_Z, respectively, one guarantees that longitudinal gauge boson self-energies are subtracted on the mass shell. Using this condition one gets [23,11]

TABLE III. Standard model differential cross section in pb for the α and the G_μ scheme.

θ (deg)	$\left(\frac{d\sigma}{d\cos\theta}\right)_0$ (200GeV) α scheme	$\left(\frac{d\sigma}{d\cos\theta}\right)_0$ (200GeV) G_μ scheme	Difference $\delta\sigma$
10	155.6123	175.3002	-0.1123
30	106.9359	120.4653	-0.1123
50	59.3622	66.8726	-0.1123
70	33.5360	37.7789	-0.1123
90	20.5578	23.1588	-0.1123
110	13.7370	15.4749	-0.1123
130	9.8762	11.1258	-0.1123
150	7.6402	8.6069	-0.1123
170	6.5744	7.4062	-0.1123
180	6.4424	7.2575	-0.1123

$$\frac{\delta M_W^2}{M_W^2} - \frac{\delta M_Z^2}{M_Z^2} = -\frac{g^2}{16\pi^2}(4s_W^2)\,\triangle - \delta\chi, \tag{25}$$

where $\delta\chi$ is the finite part given by [$R_1 = M_Z^2/M_W^2$, $R_2 = m_{H_1^0}^2/M_W^2$]

$$\begin{aligned}\delta\chi = \frac{g^2}{16\pi^2}\Bigg(& (3-4s_W^2)\int_0^1 dx \ln[1-x(1-x)R_1] \\ & -\frac{1}{2c_W^2}\int_0^1 dx \ln[x^2R_1 + (1-x)R_2] + 4s_W^2 \\ & -(3-\tfrac{1}{2}t_W^2 + 2s_W^2)\int_0^1 dx \ln[x^2 + (1-x)R_1] \\ & +\left(\frac{1}{2}\right)\int_0^1 dx \ln[x^2 + (1-x)R_2]\Bigg).\end{aligned} \tag{26}$$

The above expression is the same as in QFD [23,11] since we are working in the Wess-Zumino gauge. As was mentioned before, supersymmetry does not alter the ghost sector in this gauge [18].

Now we turn to the determination of δZ_A, δZ_W, and δZ_Z in terms of self-energies of gauge bosons. To this end we denote the bare self-energies of the photon (γ), $W^{\pm}$, Z, and the γZ mixing amplitudes by $\pi^{\gamma}(q^2)g_{\mu\nu} + \cdots, a^C(q^2)g_{\mu\nu} + \cdots$, respectively, where ($C = W$, Z, γZ). Subtracting the gauge boson self-energies on-shell, the renormalized self-energies are [23,11]

$$\tilde{\pi}^{\gamma}(q^2) = \pi^{\gamma}(q^2) - \pi^{\gamma}(0), \tag{27}$$

$$\tilde{a}^C(q^2) = a^C(q^2) - a^C(M_C^2) - \delta Z_C(q^2 - M_C^2), \tag{28}$$

where $C = W, Z$. From these relations the field renormalization constants δZ_A, δZ_W, and δZ_Z are found to be

$$\delta Z_A = \pi^{\gamma}(0), \tag{29}$$

$$\delta Z_W = \pi^{\gamma}(0) + Y_{WZ}\cot^2\theta_W, \tag{30}$$

$$\delta Z_Z = \pi^{\gamma}(0) + Y_{WZ}(\cot^2\theta_W - 1), \tag{31}$$

where

$$Y_{WZ} = \frac{a^W(M_W^2)}{M_W^2} - \frac{a^Z(M_Z^2)}{M_Z^2} + \frac{\delta M_W^2}{M_W^2} - \frac{\delta M_Z^2}{M_Z^2}. \tag{32}$$

We note that in the OMSRS [23,11] the photon does not carry an independent wave-function renormalization.

In order to determine δZ_R, δZ_L, δg, and $\delta g'$ one must first calculate the neutrino and the electron self-energies. The counterterms δg and $\delta g'$ are determined by requiring that the photon-lepton-lepton vertex defines the physical or the renormalized charge, Fig. 2. The charge thus defined must then be independent of the lepton mass m which means that δg and $\delta g'$ must be independent of the lepton mass; otherwise, the renormalized charge would be different for the muon and the electron and our renormalization procedure would fail. For this consistency check, all terms involving powers of m^2/M_W^2 were retained [23,11]. The Thomson charge was shown to be independent of mass in SQFD [11].

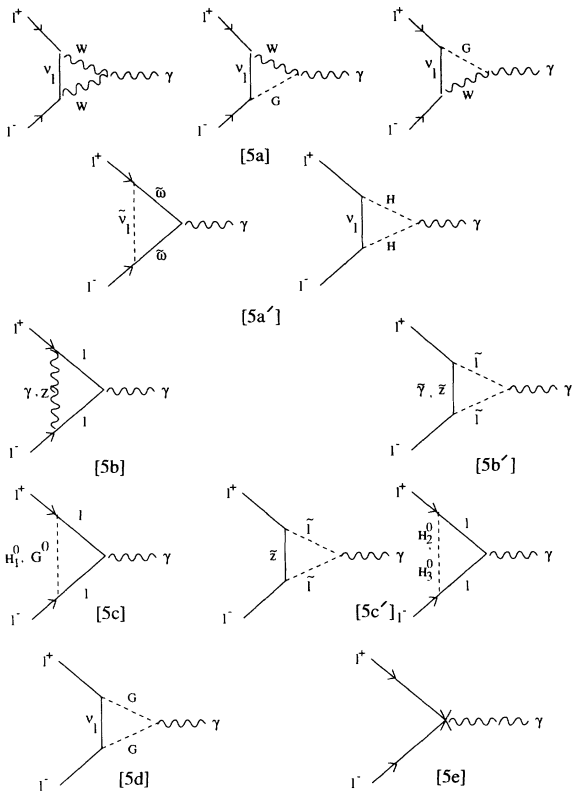

FIG. 2. Diagrams needed to arrive at the definition of the Thomson charge, i.e., to determine the counterterms δg and $\delta g'$. These are the one particle irreducible diagrams contributing to the lepton-lepton-photon vertex.

We follow Sakakibara [23] and choose to determine δZ_L by subtracting the left-handed fermion ($T_3 = +1/2$) on the mass shell. Similarly δZ_R is fixed by subtracting the right-handed fermion ($T_3 = 0$) on the mass shell. This implies that the neutrino must be subtracted on shell. The self-energy diagrams of the neutrino are given in Fig. 3. The contribution of each is listed in Appendix A. From these one easily determines δZ_L since [23,11]

$$\delta Z_L = \nu(0). \tag{33}$$

The contributions of the standard particles to the neutrino self-energy agree with Sakakibara [23], thus providing a check on our calculations.

Since the electron is both left- and right-handed in SQFD, the left handed coming in doublet with the neutrino, and we have already fixed δZ_L by subtracting the neutrino on the mass shell we must attach to each electron a finite piece f_L [23,11]. The right-handed electron is subtracted on shell.

Calculating the electron self-energy diagrams given in Fig. 4, and using the definitions [23,11]

$$\delta Z_R = \sigma_{R0} + 2\sigma_{R1} + 2\rho_1, \tag{34}$$

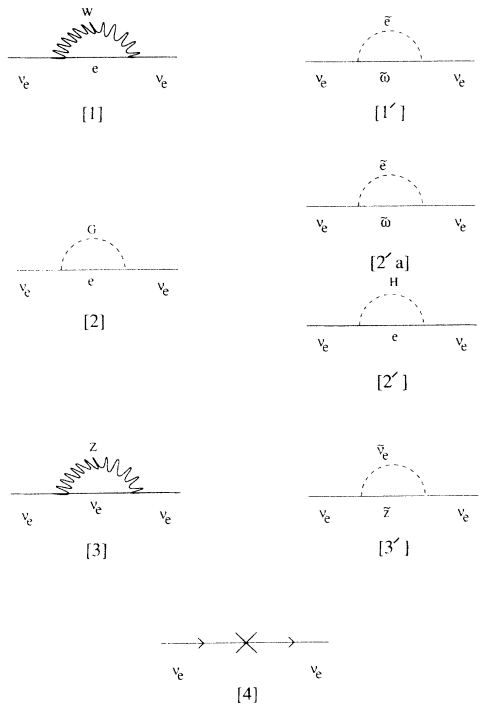

FIG. 3. One loop Feynman diagrams contributing to the neutrino self-energy in SQFD.

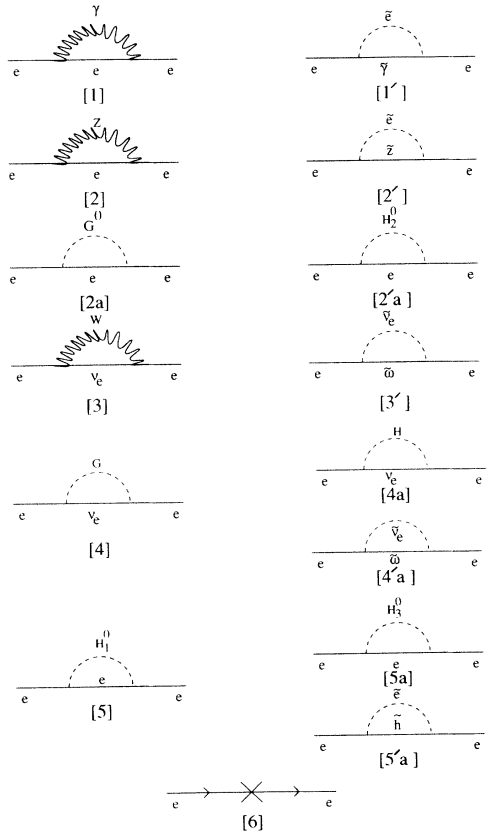

FIG. 4. One loop Feynman diagrams contributing to the electron self-energy in SQFD.

$$f_L = -\delta Z_L + \sigma_{L0} + 2\sigma_{L1} + 2\rho_1, \tag{35}$$

we extract δZ_R and f_L. We find that [11] f_L is finite in SQFD. Now turning to the lepton-lepton-photon vertex corrections, we find

$$\delta Z_R^C + \Lambda_R^C = 0, \tag{36}$$

where $C = Z, \gamma, H_1^0, G^0, G^+, \tilde{z}, \tilde{\gamma}, H_2^0, H_3^0, H^+, \tilde{h}, \tilde{\omega}$, and

$$\begin{aligned}
f_L^W + \delta Z_L^W + \Lambda_L^W &= \frac{g^2}{16\pi^2}\triangle, \\
f_L^Z + f_L^\gamma + \delta Z_L^Z + \Lambda_L^Z + \Lambda_L^\gamma &= 0, \\
f_L^{G^0} + f_L^{H_1^0} + \delta Z_L^{G^+} + \Lambda_L^{G^0} + \Lambda_L^{H_1^0} &= 0, \\
f_L^{H_2^0} + f_L^{H_3^0} + \delta Z_L^{H^+} + \Lambda_L^{H_2^0} + \Lambda_L^{H_3^0} &= 0, \\
f_L^{\tilde{\omega}} + \delta Z_L^{\tilde{\omega}} + \Lambda_L^{\tilde{\omega}} &= 0, \\
f_L^{\tilde{z}} + f_L^{\tilde{\gamma}} + \delta Z_L^{\tilde{z}} + \Lambda_L^{\tilde{z}} + \Lambda_L^{\tilde{\gamma}} &= 0, \\
f_L^{\tilde{z}} + f_L^{\tilde{h}} + \delta Z_L^{\tilde{\omega}} + \Lambda_L^{\tilde{z}} + \Lambda_L^{\tilde{h}} &= 0,
\end{aligned} \tag{37}$$

where Λ_L and Λ_R are defined via

$$-ie\gamma^\mu\Big(\frac{1-\gamma_5}{2}\Big)\Lambda_L - ie\gamma^\mu\Big(\frac{1+\gamma_5}{2}\Big)\Lambda_R. \tag{38}$$

Summing over all contributions, Eqs. (36) and (37) may be written as

$$\delta Z_R + \Lambda_R = 0, \tag{39}$$

$$f_L + \delta Z_L + \Lambda_L = \frac{g^2}{16\pi^2}\,\triangle\,. \tag{40}$$

The counterterm diagram 5 e in Fig. 12 gives

$$\begin{aligned}
\Lambda_R^c &= \delta Z_R + \frac{\delta g'}{e}\cos\theta_W, \\
\Lambda_L^c &= \delta Z_L + \frac{\delta g}{2g} + \frac{\delta g'}{2g}\cot\theta_W.
\end{aligned} \tag{41}$$

Our renormalization condition requires [23,11]

$$\begin{aligned}
\Lambda_R + \delta Z_R + \frac{\delta g'}{e}\cos\theta_W &= 0, \\
f_L + \Lambda_L + \delta Z_L + \frac{\delta g}{2g} + \frac{\delta g'}{2g}\cot\theta_W &= 0.
\end{aligned} \tag{42}$$

Together with Eqs. (39) and (40) this implies

$$\delta g' = 0, \tag{43}$$

$$\frac{\delta g}{2g} = -\frac{g^2}{16\pi^2}\,\triangle\,. \tag{44}$$

In calculating the one loop corrections to $e^+e^- \longrightarrow W^+W^-$ in SQFD one encounters a large number of Feynman diagrams. A systematic procedure was pioneered by Passarino and Veltman [24] to deal with this plethora of integrals. Using this approach we must evaluate in dimensional regularization scheme integrals of the type

$$A(m) = -\frac{1}{i\pi^2}\int d^n q \frac{1}{[q^2 - m^2]}, \tag{45}$$

$$B_0; B_\mu; B_{\mu\nu} = \frac{1}{i\pi^2}\int d^n q \frac{1; q_\mu; q_\mu q_\nu}{[q^2 - m_1^2][(q+k)^2 - m_2^2]}, \tag{46}$$

$$C_0; C_\mu; C_{\mu\nu}; C_{\mu\nu\alpha} = -\frac{1}{i\pi^2}\int d^n q \frac{1; q_\mu; q_\mu q_\nu; q_\mu q_\nu q_\alpha}{[q^2 - m_1^2][(q+k)^2 - m_2^2][(q+p_5)^2 - m_3^2]}, \tag{47}$$

where $p_5 = k + p$,

$$D_0; D_\mu; D_{\mu\nu}; D_{\mu\nu\alpha} = \frac{1}{i\pi^2}\int d^n q \frac{1; q_\mu; q_\mu q_\nu; q_\mu q_\nu q_\alpha}{[q^2 - m_1^2][(q+k)^2 - m_2^2][(q+k+p)^2 - m_3^2][(q+k+p+l)^2 - m_4^2]}. \tag{48}$$

Every such one loop integral can be decomposed in terms of form factors [24,11]. For example consider C_μ which can be written as

$$C_\mu = C_{11} k_\mu + C_{12} p_\mu.$$

After some algebra one can express C_{11} and C_{12} in terms of the scalar integrals C_0 and three different B_0's [24,11]. In this manner one can iteratively express all the invariant functions $B_1, \ldots, B_{22}, C_{11}, \ldots, C_{36}, D_{11}, \ldots, D_{313}$ in terms of the scalar integrals A, B_0, C_0, and D_0. General expressions for these scalar integrals were given in terms of logarithms and spence functions by 't Hooft and Veltman [25]. The explicit details of this procedure may be found in [25,11]. In [11] (we mean here notes of our thesis cited in [11]) we have also given the complete expressions for the infrared (IR) singular integrals and other relevant integrals encountered. One great advantage of the above procedure is that it allows a consistency check on the computer program, since some integrals such as C_{23}, C_{34}, are computed in two different ways [24,11]. In this manner we have obtained numerical consistency up to at least eight decimal places.

V. THE SELF-ENERGY AND THE WAVE-FUNCTION RENORMALIZATION CONTRIBUTION TO THE ONE LOOP DIFFERENTIAL CROSS SECTION

In this section we give the contribution of the self-energy insertions and the wave-function renormalization [WFR] to the one loop differential cross section.

Consider first the neutrino contribution [Fig. 5(a)]. Contracting this with the tree-level amplitude one has

$$\left(\frac{d\sigma}{d\cos\theta}\right)_1^\nu = 2\tilde{\nu}(t)\Phi[-(a_s a_t + b_s b_t)\mathcal{A}_{st} + (a_t^2 + b_t^2)\mathcal{A}_{tt}]. \tag{49}$$

We note that the subscript 1 in the expression for the differential cross section is used to indicate and emphasize that we are working to the one loop order. This notation is used in this and our other two papers [19,20].

The renormalized neutrino self-energy $\tilde{\nu}$ in the above expression is defined as

$$\tilde{\nu}(k^2) = \nu(k^2) - \nu(0). \tag{50}$$

Ignoring the terms proportional to the electron mass, for QFD one has

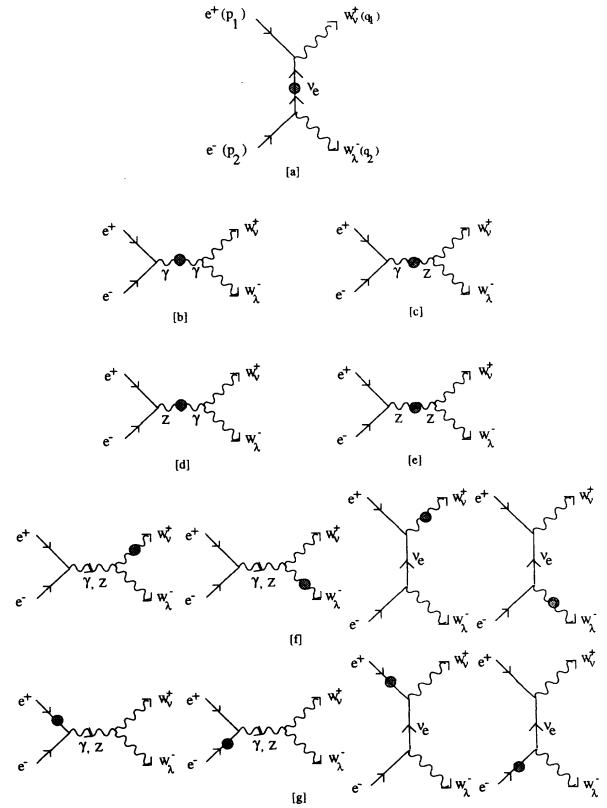

FIG. 5. Feynman diagrams for self-energy and wave-function corrections.

TABLE IV. Neutrino self-energy contribution to one loop radiative corrections in pb for center-of-mass energy of 200 GeV.

θ(deg)	$\left(\frac{d\sigma}{d\cos\theta}\right)_1^{\rm QFD}$	$\left(\frac{d\sigma}{d\cos\theta}\right)_1^{\rm SP}$	$\left(\frac{d\sigma}{d\cos\theta}\right)_1^{\rm SQFD}$
10	+0.0346	+0.4416	+0.4762
30	+0.0491	+0.4162	+0.4653
50	+0.0552	+0.3215	+0.3767
70	+0.0565	+0.2550	+0.3115
90	+0.0568	+0.2170	+0.2738
110	+0.0569	+0.1951	+0.2520
130	+0.0568	+0.1812	+0.2380
150	+0.0563	+0.1722	+0.2285
170	+0.0559	+0.1676	+0.2235
180	+0.0559	+0.1670	+0.2229

TABLE V. Electron WFR contribution to one loop radiative corrections in pb for center-of-mass energy of 200 GeV.

θ (deg)	$(\frac{d\sigma}{d\cos\theta})_1^{\rm QFD}$	$(\frac{d\sigma}{d\cos\theta})_1^{\rm SP}$	$(\frac{d\sigma}{d\cos\theta})_1^{\rm SQFD}$
10	-5.2997	+0.4867	-4.8130
30	-3.6883	+0.3341	-3.3542
50	-2.1070	+0.1850	-1.9220
70	-1.2545	+0.1040	-1.1505
90	-0.8252	+0.0633	-0.7619
110	-0.5945	+0.0419	-0.5526
130	-0.4574	+0.0299	-0.4275
150	-0.3733	+0.0230	-0.3503
170	-0.3315	+0.0197	-0.3118
180	-0.3263	+0.0193	-0.3070

$$\begin{aligned}\tilde{\nu}(k^2) = &-[B_0(M_W, m_e, k^2) - B_0(M_W, m_e, 0) \\ &+B_1(M_W, m_e, k^2) - B_1(M_W, m_e, 0)] - (1/2c_W^2)[B_0(M_Z, m_{\nu_e}, k^2) \\ &-B_0(M_Z, m_{\nu_e}, 0) + B_1(M_Z, m_{\nu_e}, k^2) - B_1(M_Z, m_{\nu_e}, 0)],\end{aligned} \tag{51}$$

and for SQFD, in addition to the above contribution from QFD,

$$\tilde{\nu}(k^2) = [B_1(m_{\tilde{\omega}}, m_{\tilde{e}}, k^2) - B_1(m_{\tilde{\omega}}, m_{\tilde{e}}, 0)] + (1/2c_W^2)[B_1(m_{\tilde{z}}, m_{\tilde{\nu_e}}, k^2) - B_1(m_{\tilde{z}}, m_{\tilde{\nu_e}}, 0)]. \tag{52}$$

We recall that $\doteq$ is equivalent to $= \frac{g^2}{16\pi^2}$. The numerical values for $\left(\frac{d\sigma}{d\cos\theta}\right)_1^{\nu}$ are listed in Table IV for CM energy of 200 GeV and various CM angles. We note that $\left(\frac{d\sigma}{d\cos\theta}\right)_1^{\rm QFD}$ in the second column in Table IV represents the QFD contribution to the one loop (hence the subscript 1) differential cross section. Similarly $\left(\frac{d\sigma}{d\cos\theta}\right)_1^{\rm SP}$ in the third column in Table IV represents the SP contribution to the one loop differential cross section. Finally the last column represents the total contribution in SQFD.

The W-boson WFR [Fig. 5(f)] contribution is

$$\left(\frac{d\sigma}{d\cos\theta}\right)_1^{W} = \Phi\mathcal{A}_0\left[\left(\frac{\partial\tilde{a}^W(s_3)}{\partial s_3}\right)_{s_3=M_W^2} + \left(\frac{\partial\tilde{a}^W(s_4)}{\partial s_4}\right)_{s_4=M_W^2}\right]. \tag{53}$$

The renormalized derivative of $\tilde{a}^W$ is easily obtained from the definition in Sec. IV [Eq. (28)] and the results for the self-energy contributions listed in Appendix E. The numerical values for Eq. (53) are given in Table VI. We note that the infrared infinite part in this expression, which is given in Appendix E, Eq. (E11), is cancelled against the corresponding bremsstrahlung contribution [see next section]. What is then given in Table VI is the finite piece. We also note that in Table VI the first entry in the QFD column is for the Higgs boson mass of 100 GeV, the second entry in the same column corresponds to a Higgs boson mass of 50 GeV. The first and second entry in the SP column corresponds to with and without a mass splitting term,[5] respectively. To get the total contribution in context of SQFD (i.e, third column) we have added the second entry in the first column (i.e, Higgs boson mass of 50 GeV) to both entries in the second column, the reason being that we have assumed a 50 GeV Higgs boson mass in SQFD.

The self-energy insertions from Figs. 5(b)–5(e) are successively written as

TABLE VI. W-boson WFR contribution to one loop radiative corrections in pb for center-of-mass energy of 200 GeV.

θ (deg)	$\left(\frac{d\sigma}{d\cos\theta}\right)_1^{\rm QFD}$	$\left(\frac{d\sigma}{d\cos\theta}\right)_1^{\rm SP}$	$\left(\frac{d\sigma}{d\cos\theta}\right)_1^{\rm SQFD}$
10	+3.2802,+3.0756	-10.1466,-8.8322	-7.0735,-5.7566
30	+2.2542,+2.1135	-6.9744,-6.0694	-4.8609,-3.9559
50	+1.2513,1.1733	-3.8716,-3.3693	-2.6983,-2.1960
70	+0.7069,+0.6628,	-2.1872,-1.9034	-1.5244,-1.2406
90	+0.4333,+0.4063	-1.3408,-1.1668	-0.9345,-0.7605
110	+0.2896,+0.2715	-0.8959,-0.7797	-0.6244,-0.5082
130	+0.2082,+0.1952	-0.6441,-0.5606	-0.4489,-0.3654
150	+0.1611,+0.1510	-0.4983,-0.4336	-0.3473,-0.2826
170	+0.1386,+0.1299	-0.4288,-0.3731	-0.2989,-0.2432
180	+0.1358,+0.1273	-0.4202,-0.3657	-0.2929,-0.2384

[5]When supersymmetry is broken a logarithmic infinity remains in the wave-function renormalization of the W, this term is proportional to $[2s_W^2(m_{\tilde{\gamma}}^2/M_W^2) + 2c_W^2(m_{\tilde{z}}^2/M_W^2) + 2(m_{\tilde{\omega}}^2/M_W^2) - 4c_W(m_{\tilde{z}}m_{\tilde{\omega}}/M_W^2)]\triangle$. We note that the above term is zero in the SUSY limit, [$m_{\tilde{\gamma}} = m_\gamma = 0$, $m_{\tilde{z}} = M_Z$, $m_{\tilde{\omega}} = M_W$]. "With mass splitting refers to the case when this term is subtracted by means of a counterterm which contains also finite pieces." Without mass splitting term refers to the case when subtraction is made without the introduction of any finite terms.

TABLE VII. γ self-energy contribution to one loop radiative corrections in pb for center-of-mass energy of 200 GeV.

θ (deg)	$\left(\frac{d\sigma}{d\cos\theta}\right)_1^{\rm QFD}$	$\left(\frac{d\sigma}{d\cos\theta}\right)_1^{\rm SP}$	$\left(\frac{d\sigma}{d\cos\theta}\right)_1^{\rm SQFD}$
10	+2.8626	-0.0032	+2.8594
30	+1.0384	-0.0011	+1.0373
50	-0.0320	+0.00004	-0.0320
70	-0.5000	+0.0006	-0.4994
90	-0.7012	+0.0008	-0.7004
110	-0.7844	+0.0009	-0.7835
130	-0.8143	+0.0009	-0.8134
150	-0.8218	+0.0009	-0.8209
170	-0.8224	+0.0009	-0.8215
180	-0.8223	+0.0009	-0.8214

TABLE VIII. γ-Z self-energy contribution to one loop radiative corrections in pb for center-of-mass energy of 200 GeV.

θ (deg)	$\left(\frac{d\sigma}{d\cos\theta}\right)_1^{\rm QFD}$	$\left(\frac{d\sigma}{d\cos\theta}\right)_1^{\rm SP}$	$\left(\frac{d\sigma}{d\cos\theta}\right)_1^{\rm SQFD}$
10	+0.0152,+0.0181	+0.0966,+0.3222	+0.1147,+0.3403
30	+0.0055,+0.0066	+0.0350,+0.1169	+0.0416,+0.1235
50	-0.0002,-0.0002	-0.0011,-0.0036	-0.0013,-0.0038
70	-0.0027,-0.0032	-0.0169,-0.0563	-0.0201,-0.0595
90	-0.0037,-0.0044	-0.0237,-0.0789	-0.0281,-0.0833
110	-0.0042,-0.0050	-0.0265,-0.0883	-0.0315,-0.0933
130	-0.0043,-0.0051	-0.0265,-0.0916	-0.0316,-0.0967
150	-0.0044,-0.0052	-0.0277,-0.0925	-0.0329,-0.0977
170	-0.0044,-0.0052	-0.0277,-0.0926	-0.0329,-0.0978
180	-0.0044,-0.0052	-0.0277,-0.0926	-0.0329,-0.0978

$$\left(\frac{d\sigma}{d\cos\theta}\right)_1^{\gamma\gamma} = 2\Phi\frac{s_W^2}{s^2}[a_s\mathcal{A}_{ss} - a_t\mathcal{A}_{st}]\tilde{\pi}^{\gamma}(s), \tag{54}$$

$$\left(\frac{d\sigma}{d\cos\theta}\right)_1^{\gamma Z} = 2\Phi\frac{s_W c_W}{[s][s-M_Z^2]}[a_s\mathcal{A}_{ss} - a_t\mathcal{A}_{st}]\tilde{a}^{\gamma Z}(s), \tag{55}$$

$$\left(\frac{d\sigma}{d\cos\theta}\right)_1^{Z\gamma} = 2\Phi\frac{s_W}{[4c_W][s][s-M_Z^2]}\{[a_s(1-4s_W^2)-b_s]\mathcal{A}_{ss} - [a_t(1-4s_W^2)-b_t]\mathcal{A}_{st}\}\tilde{a}^{Z\gamma}(s), \tag{56}$$

$$\left(\frac{d\sigma}{d\cos\theta}\right)_1^{ZZ} = 2\Phi\frac{1}{4[s-M_Z^2]^2}\{[a_s(1-4s_W^2)-b_s]\mathcal{A}_{ss} - [a_t(1-4s_W^2)-b_t]\mathcal{A}_{st}\}\tilde{a}^{Z}(s). \tag{57}$$

The renormalized a (i.e., $\tilde{a}^{\gamma-Z}$) of the γ-Z self-energy insertion is given by

$$\tilde{a}^{\gamma-Z}(s) = a^{\gamma-Z}(s) - Y_{WZ}\cot\theta_W + t_W M_W^2\frac{\delta g}{g}. \tag{58}$$

The numerical values for Eqs. (54)–(57) are listed respectively in Tables VII, VIII, IX, and X. We note that in Tables VII, IX, and X the first entry in the QFD column is for the Higgs boson mass of 100 GeV; the second entry in the same column corresponds to a Higgs boson mass of 50 GeV. The first and second entry in the SP column corresponds to having and not having a mass splitting term respectively. To get the total contribution in context of SQFD (i.e., third column) we have added the second entry in the first column (i.e, Higgs boson mass of 50 GeV) to both the entries in the second column, the reason being that we have assumed a 50 GeV Higgs boson mass in SQFD.

Now we turn to the contribution by the electron WFR to the one-loop-corrected cross section [Fig. 5(g)]. This is given by

$$\left(\frac{d\sigma}{d\cos\theta}\right)_1^{e} = \left(\frac{d\sigma}{d\cos\theta}\right)_1^{e_L} + \left(\frac{d\sigma}{d\cos\theta}\right)_{1fct}^{e^+e^-\gamma+e^+e^-Z,e_R}, \tag{59}$$

where

TABLE IX. Z-γ self-energy contribution to one loop radiative corrections in pb for center-of-mass energy of 200 GeV.

θ (deg)	$\left(\frac{d\sigma}{d\cos\theta}\right)_1^{\rm QFD}$	$\left(\frac{d\sigma}{d\cos\theta}\right)_1^{\rm SP}$	$\left(\frac{d\sigma}{d\cos\theta}\right)_1^{\rm SQFD}$
10	+0.0059,+0.0070	+0.0375,+0.1251	+0.0445,+0.1321
30	+0.0025,+0.0030	+0.0158,+0.0528	+0.0188,+0.0558
50	+0.0005,+0.0006	+0.0033,+0.0109	+0.0039,+0.0115
70	-0.0003,-0.0003	-0.0021,-0.0067	-0.0024,-0.0070
90	-0.0007,-0.0008	-0.0044,-0.0147	-0.0052,-0.0155
110	-0.0009,-0.0010	-0.0055,-0.0183	-0.0065,-0.0193
130	-0.0010,-0.0011	-0.0061,-0.0203	-0.0072,-0.0214
150	-0.0010,-0.0012	-0.0065,-0.0215	-0.0077,-0.0227
170	-0.0010,-0.0012	-0.0066,-0.0222	-0.0078,-0.0234
180	-0.0011,-0.0013	-0.0067,-0.0223	-0.0080,-0.0236

TABLE X. Z-boson self-energy contribution to one loop radiative corrections in pb for center-of-mass energy of 200 GeV.

θ (deg)	$\left(\frac{d\sigma}{d\cos\theta}\right)_1^{\rm QFD}$	$\left(\frac{d\sigma}{d\cos\theta}\right)_1^{\rm SP}$	$\left(\frac{d\sigma}{d\cos\theta}\right)_1^{\rm SQFD}$
10	+1.8726,+1.9374	-0.1438,+0.0706	+1.7936,+2.0080
30	+0.7903,+0.8177	-0.0607,+0.0298	+0.7570,+0.8475
50	+0.1636,+0.1693	-0.0126,+0.0061	+0.1567,+0.1754
70	-0.1043,-0.1079	+0.0080,-0.0039	-0.0999,-0.1118
90	-0.2200,-0.2276	+0.0169,-0.0083	-0.2107,-0.2359
110	-0.2745,-0.2840	+0.0211,-0.0103	-0.2629,-0.2943
130	-0.3043,-0.3148	+0.0234,-0.0115	-0.2914,-0.3263
150	-0.3224,-0.3336	+0.0248,-0.0121	-0.3088,-0.3457
170	-0.3317,-0.3431	+0.0255,-0.0125	-0.3176,-0.3556
180	-0.3328,-0.3444	+0.0256,-0.0125	-0.3188,-0.3569

$$\left(\frac{d\sigma}{d\cos\theta}\right)_1^{e_L} = \Phi f_L[(a_s-b_s)^2\mathcal{A}_{ss} - 2(a_t-b_t)(a_s-b_s)\mathcal{A}_{st} + (a_t-b_t)^2\mathcal{A}_{tt}], \tag{60}$$

$$\left(\frac{d\sigma}{d\cos\theta}\right)_{1fct}^{e^+e^-\gamma+e^+e^-Z,e_R} = \Phi\delta\bar{Z}_R{}^{\gamma}[(a_s+b_s)^2\mathcal{A}_{ss} - 2(a_t+b_t)(a_s+b_s)\mathcal{A}_{st} + (a_t+b_t)^2\mathcal{A}_{tt}]. \tag{61}$$

A few remarks are in order to clarify the appearance of the right-handed electron term in the electron WFR contribution [see Eq. (59)]. As mentioned in the previous section the right-handed electron is subtracted on shell and does not contribute. The right-handed term in Eq. (59) comes from the counterterm contribution considered in [19]. This is why we have labeled it with the names of the relevant vertices from which it arises. fct stands for the finite parts of the counterterms [19]. We have included it here in the electron WFR term because we need it for the infrared cancellations considered in the next section. δZ_R is written with a bar since the quadratic divergence in it has been canceled in [19]. The superscript γ appearing on δZ_R indicates that only the photon's contribution to δZ_R has been considered here. The quantity f_L can be easily extracted by using the definition of f_L given in Sec. IV and the expressions for the electron self-energy given in Appendix B. For the case of QFD one finds

$$f_L \doteq -s_W^2\left[\frac{9}{2} + \ln\frac{M_Z^2}{m_e^2} + 2\ln\left(\frac{\lambda^2}{m_e^2}\right)\right], \tag{62}$$

$$\delta\bar{Z}_R{}^{\gamma} \doteq -s_W^2\left[4 + 2\ln\left(\frac{\lambda^2}{m_e^2}\right)\right]. \tag{63}$$

For the case of SQFD, in addition to the above, one has (we note that $2a_1^2/c_W^2 = [1-2s_W^2]^2/2c_W^2$, see Appendix B for a definition of a_1),

$$f_L^S \doteq +\frac{2a_1^2}{c_W^2}[B_1(m_{\tilde{z}},m_{\tilde{e}},m_e^2)] + 2s_W^2[B_1(m_{\tilde{\gamma}},m_{\tilde{e}},m_e^2)] + [B_1(m_{\tilde{\omega}},m_{\tilde{\nu_e}},m_e^2)] - [B_1(m_{\tilde{\omega}},m_{\tilde{e}},0)] - \frac{1}{2c_W^2}[B_1(m_{\tilde{z}},m_{\tilde{\nu_e}},0)]. \tag{64}$$

This [Eq. (64)] reduces in the SUSY limit to

$$f_L^S \doteq -s_W^2\left[-\frac{1}{2} + \ln\frac{M_Z^2}{m_e^2}\right]. \tag{65}$$

The numerical results for the electron WFR are listed in Table V.

VI. BREMSSTRAHLUNG

As is well known, in order to obtain finite cross sections, in the limit of vanishing photon mass, we have to include emission of real photons by the external charged particles. Since the photon interacts both with the electron and the W boson the relevant bremsstrahlung diagrams are displayed in Fig. 6. The charged would-be Goldstone boson, which is a longitudinal mode of the W boson in the 't Hooft–Feynman gauge, must also be included as in Fig. 6.

In the soft photon approximation (i.e., the emission of photons with small energy) we obtain, with the help of the Ward identity [12,11] and the assumption that the W's be on mass shell, the usual factorization of the bremsstrahlung cross section [12]:

$$\frac{d\sigma_B}{d\cos\theta} = \frac{d\sigma_0}{d\cos\theta}\delta_B. \tag{66}$$

Here

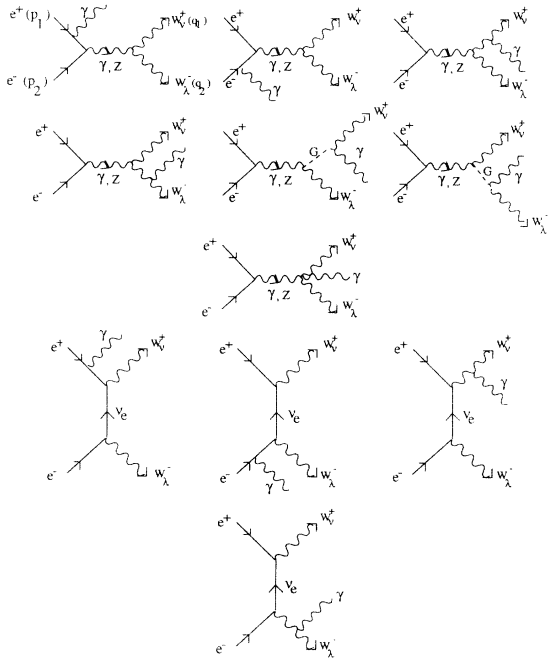

FIG. 6. Diagrams for the process $e^+e^- \longrightarrow W^+W^-\gamma$.

$$\delta_B = \delta_e + \delta_W + \delta_t + \delta_u, \tag{67}$$

$$\delta_e = -\left(\frac{\alpha}{\pi}\right)\left[\ln\left(\frac{s}{\lambda^2}\right) - \ln\left(\frac{s}{\lambda^2}\right)\ln\left(\frac{s}{m_e^2}\right) + \ln(a^2) - \ln(a^2)\ln\left(\frac{s}{m_e^2}\right) + \frac{1}{2}\ln^2\left(\frac{m_e^2}{s}\right) + \ln\left(\frac{m_e^2}{s}\right) + \frac{\pi^2}{3}\right], \tag{68}$$

$$\begin{aligned}\delta_W = -\left(\frac{\alpha}{\pi}\right)\Big\{&\ln\left(\frac{s}{\lambda^2}\right) + \frac{s-2M_W^2}{s\beta_W}\ln\left(\frac{s}{\lambda^2}\right)\ln\left(\frac{1-\beta_W}{1+\beta_W}\right) + \ln(a^2) \\ &+\frac{s-2M_W^2}{s\beta_W}\ln(a^2)\ln\left(\frac{1-\beta_W}{1+\beta_W}\right) + \frac{1}{\beta}\ln\left(\frac{1-\beta_W}{1+\beta_W}\right) - \frac{s-2M_W^2}{s\beta_W}\Big[2\mathrm{Sp}\left(\frac{1-\beta_W}{1+\beta_W}\right) \\ &-\frac{1}{2}\ln^2\left(\frac{1-\beta_W}{1+\beta_W}\right) - \frac{\pi^2}{3} + 2\ln\left(\frac{1-\beta_W}{1+\beta_W}\right)\ln\left(\frac{2\beta_W}{1+\beta_W}\right)\Big]\Big\},\end{aligned} \tag{69}$$

$$\begin{aligned}\delta_t = -\left(\frac{\alpha}{\pi}\right)\Big\{&-2\ln\left(\frac{-t}{\lambda^2}\right)\ln\left(\frac{M_W^2-t}{m_e M_W}\right) - 2\ln\left(\frac{s}{-t}\right)\ln\left(\frac{M_W^2-t}{m_e M_W}\right) \\ &-2\ln(a^2)\ln\left(\frac{M_W^2-t}{m_e M_W}\right) + 2\Big[\mathrm{Sp}\left(1-\frac{1}{2}\frac{s(1-\beta_W)}{M_W^2-t}\right) + \mathrm{Sp}\left(1-\frac{1}{2}\frac{s(1+\beta_W)}{M_W^2-t}\right)\Big]\Big\},\end{aligned} \tag{70}$$

$$\begin{aligned}\delta_u = -\left(\frac{\alpha}{\pi}\right)\Big\{&2\ln\left(\frac{-u}{\lambda^2}\right)\ln\left(\frac{M_W^2-u}{m_e M_W}\right) + 2\ln\left(\frac{s}{-u}\right)\ln\left(\frac{M_W^2-u}{m_e M_W}\right) \\ &+2\ln(a^2)\ln\left(\frac{M_W^2-u}{m_e M_W}\right) - 2\Big[\mathrm{Sp}\left(1-\frac{1}{2}\frac{s(1-\beta_W)}{M_W^2-u}\right) + \mathrm{Sp}\left(1-\frac{1}{2}\frac{s(1+\beta_W)}{M_W^2-u}\right)\Big]\Big\},\end{aligned} \tag{71}$$

$$\begin{aligned} a &= \frac{2\triangle E_b}{\sqrt{s}}, \\ &= \frac{\triangle E_b}{E_b}. \end{aligned} \tag{72}$$

The subscript B indicates that this is the bremsstrahlung contribution to δ, while subscript b as previously mentioned corresponds to the beam energy.

To the best of our knowledge, the only other places the complete expression for the bremsstrahlung (infrared infinite) cross section of the process $e^+e^- \longrightarrow W^+W^-$ has been given are [14,15]. The above expression [Eq. (66)] agrees with [14]. We note however the misprint in [14] [second term of line 3 of Eq. (5.18)]. We summarize below the steps needed to arrive at the infrared finite expression. Consider the two infinite single logarithms terms in the electron and the W expressions [Eqs. (68) and (69)]. These are canceled by the WFR contributions of the electron and the W to the $e^+e^- \longrightarrow W^+W^-$ cross section shown in Fig. 5(f) and 5(g). The W self-energy (SE) contribution works out to be (including only the infinite part, Appendix E)

$$\frac{d\sigma^{(\mathrm{IRIV})}_{W(\mathrm{SE})}}{d\cos\theta} = -\frac{\alpha}{\pi}\left[\ln\left(\frac{\lambda^2}{M_W^2}\right)\right]\frac{d\sigma_0}{d\cos\theta}. \tag{73}$$

On adding this to the infinite single logarithm term in Eq. (69) we get

$$\frac{d\sigma_{W(\mathrm{WFR})+W(\mathrm{brem})}}{d\cos\theta} = -\frac{\alpha}{\pi}\left[\ln\left(\frac{s}{M_W^2}\right)\right]\frac{d\sigma_0}{d\cos\theta}, \tag{74}$$

which is finite. As can be inferred, the electron produces a similar contribution to the infrared infinite virtual (IRIV) (Appendix B) term,

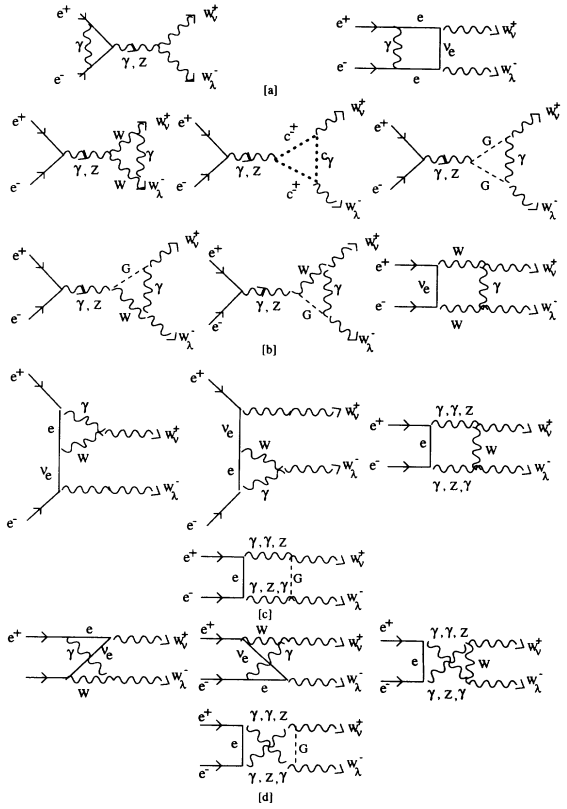

FIG. 7. Combination of diagrams which cancel the infrared infinities in the bremsstrahlung.

$$\frac{d\sigma^{(\mathrm{IRIV})}_{e(\mathrm{WFR})}}{d\cos\theta} = -\frac{\alpha}{\pi}\left[\ln\left(\frac{\lambda^2}{m_e^2}\right)\right]\frac{d\sigma_0}{d\cos\theta}, \tag{75}$$

which when considered along with the remaining single logarithmic term in Eq. (68) gives

$$\frac{d\sigma_{e(\mathrm{WFR})+e(\mathrm{brem})}}{d\cos\theta} = -\frac{\alpha}{\pi}\left[\ln\left(\frac{s}{m_e^2}\right)\right]\frac{d\sigma_0}{d\cos\theta}, \tag{76}$$

which is again finite.

The double logarithm terms in Eqs. (68)–(71) need much more work for their cancellation. Essentially certain combinations of triangle ($\triangle$) and box ($\square$) diagrams conspire to produce an effective IRIV term which cancels the corresponding infrared infinite bremsstrahlung (IRIB) term.

We start with the "simplest case," that of the triangle diagrams with two electrons and a photon as internal particles, and the box diagram with two electrons, neutrino, and a photon as the internal particles, Fig. 7(a). First consider the triangle contribution; this works out to be

$$V^{e^+e^-\gamma} + V^{e^+e^-Z}$$

$$= -2x\left(\frac{\alpha}{4\pi}\right)\Phi[(a_s^2+b_s^2)\mathcal{A}_{ss} - (a_sa_t+b_sb_t)\mathcal{A}_{st}]. \tag{77}$$

Here

$$x = 2 - 4C_{24} + 2s(C_{23}+C_{11}). \tag{78}$$

Since all C integrals can be expressed in terms of C_0 and B integrals [24,11], it can be shown that the C integrals, which are infrared divergent (IRD), are C_{11}, C_{21} and C_{31}:

$$C_{11} \simeq -C_0,\ C_{21} \simeq C_0,\ C_{31} \simeq -C_0$$

This allows us to write the IRIV contribution of Eq. (77) as

$$(V^{e^+e^-\gamma} + V^{e^+e^-Z})^{\mathrm{IRIV}} = -2\left(\frac{\alpha}{4\pi}\right)\Phi\left[2\ln\left(\frac{s}{\lambda^2}\right)\ln\left(\frac{s}{m_e^2}\right)\right][(a_s^2+b_s^2)\mathcal{A}_{ss} - (a_sa_t+b_sb_t)\mathcal{A}_{st}]. \tag{79}$$

Let us turn now to the box contribution Fig. 7(a). We know that each D_0 integral can be decomposed into a D-like term and to C_0 integrals [24]:

$$\begin{aligned}
D_0 &= \int d^nq \frac{1}{\prod_i Q_i},\\
\frac{1}{\prod_i Q_i} &= -\frac{2}{y-m_2^2-m_3^2}\left[\frac{(q+p_1).(q+p_1+p_2)}{\prod_i Q_i} - \frac{1}{2\prod_{i\neq 2}Q_i} - \frac{1}{2\prod_{i\neq 3}Q_i}\right],\\
Q_1 &= q^2 - m_1^2,\\
Q_2 &= (q+p_1)^2 - m_2^2,\\
Q_3 &= (q+p_1+p_2)^2 - m_3^2,\\
Q_4 &= (q+p_1+p_2+p_3)^2 - m_4^2,\\
y &= (p_1+p_2)^2 + p_1^2 - 2p_1(p_1+p_2).
\end{aligned} \tag{80}$$

Limiting Eq. (80) to the case of Fig. 7(a) and writing only the IRD part of D_0,

$$D_0^{\mathrm{IRD}} \simeq -\frac{2}{t}C_0^{\mathrm{IRD}}(p_2,p_1,m_e,\lambda,m_e), \tag{81}$$

the IRIV box contribution of Fig. 7(a) to the one loop cross section works out to be

$$B^{\mathrm{IRIV}}_{\gamma ee\nu_e} = \left(\frac{\alpha}{\pi}\right)\Phi\left[-\ln\left(\frac{s}{\lambda^2}\right)\ln\left(\frac{s}{m_e^2}\right)\right][(a_t^2+b_t^2)\mathcal{A}_{tt} - (a_sa_t+b_sb_t)\mathcal{A}_{st}]. \tag{82}$$

Adding both these contributions, i.e., Eqs. (79) and (82), the result is

$$\frac{d\sigma^{\mathrm{IRIV}}_{\mathrm{electron}}}{d\cos\theta} = -\frac{\alpha}{\pi}\left[\ln\left(\frac{s}{\lambda^2}\right)\ln\left(\frac{s}{m_e^2}\right)\right]\frac{d\sigma_0}{d\cos\theta}. \tag{83}$$

Using the electron part of IRIB, i.e., Eq. (68), we immediately see that the double logarithm infinity cancels between Eqs. (68) and (83).

Next we consider the contribution of diagrams shown in Fig. 7(b). The amplitude from the triangle graphs of Fig. 7(b) is reduced after a tedious calculation and some rearrangement to

$$\begin{aligned}
\mathcal{M}^{\triangle} &= \frac{ig^4}{16\pi^2}(4q_1.q_2)(s_W^2)[\bar{v}(p_1)\gamma^\mu(a_s+b_s\gamma_5)u(p_2)\Gamma_{\mu\nu\lambda}\epsilon_1^\nu\epsilon_2^\lambda]C_0^{\mathrm{IRD}}(q_1,q_2,M_W,\lambda,M_W)\\
&\quad -\frac{ig^4}{16\pi^2}\left(\frac{s_W^2}{4}\right)[\bar{v}(p_1)\gamma^\mu(1-\gamma_5)u(p_2)\Gamma^x_{\mu\nu\lambda}\epsilon_1^\nu\epsilon_2^\lambda]C_0^{\mathrm{IRD}}(q_1,q_2,M_W,\lambda,M_W),
\end{aligned} \tag{84}$$

where

$$\Gamma^x_{\mu\nu\lambda} = \Gamma_{\mu\nu\lambda} - q_{1\mu} g_{\nu\lambda}. \tag{85}$$

Amazingly the box contribution of Fig. 7(b) generates a term which exactly cancels the unwanted term in Eq. (84), i.e., the second term. Therefore,

$$\begin{aligned}\mathcal{M}^{\Box} = &-\frac{ig^4}{16\pi^2}(4q_1.q_2)(s_W^2)[\bar{v}(p_1)\not{\epsilon}_1(\not{q}_1 - \not{p}_1)\not{\epsilon}_2(a_t + b_t\gamma_5)u(p_2)]C_0^{\mathrm{IRD}}(q_1, q_2, M_W, \lambda, M_W) \\ &+\frac{ig^4}{16\pi^2}\Big(\frac{s_W^2}{4}\Big)[\bar{v}(p_1)\gamma^\mu(1-\gamma_5)u(p_2)\Gamma^x_{\mu\nu\lambda}\epsilon_1^\nu\epsilon_2^\lambda]C_0^{\mathrm{IRD}}(q_1, q_2, M_W, \lambda, M_W).\end{aligned} \tag{86}$$

Clearly the second terms in Eqs. (84) and (86) cancel each other. The remainder is precisely what we need to cancel the W-boson double logarithm infinity in Eq. (69). Since, on adding Eqs. (84) and (86) we factor out the tree-level amplitude $\mathcal{M}^{\mathcal{T}}$ [we note that $\mathcal{M}^{\mathcal{T}} = \mathcal{M}_0$],

$$\mathcal{M}^{\triangle+\Box} = \frac{\alpha}{4\pi}(4q_1.q_2)\mathcal{M}^{\mathcal{T}} C_0^{\mathrm{IRD}}(q_1, q_2, M_W, \lambda, M_W). \tag{87}$$

This yields the following cross section contribution, after substituting the infinite part of C_0:

$$\frac{d\sigma^{\mathrm{IRIV}}_{W\ \mathrm{boson}}}{d\cos\theta} = \frac{\alpha}{\pi}\frac{s - 2M_W^2}{s\beta_W}\ln\Big(\frac{s}{\lambda^2}\Big)\ln\Big(\frac{1-\beta_W}{1+\beta_W}\Big)\frac{d\sigma_0}{d\cos\theta}. \tag{88}$$

Once again this cancels the double logarithm infinity in IRIB, see Eq. (69).

Now we turn to the diagrams of Fig. 7(c), i.e., the t channel IRIV diagrams. The amplitude for the triangle diagrams is (infrared parts only)

$$\mathcal{M}_{t1} = -ig^2\Big(\frac{\alpha}{4\pi}\Big)\bar{v}(p_1)[V^x_{11}\not{\epsilon}_1(\not{q}_1 - \not{p}_1)\not{\epsilon}_2 + V^x_{13}(p_1.\epsilon_1)\not{\epsilon}_2](a_t + b_t\gamma_5)u(p_2), \tag{89}$$

$$\mathcal{M}_{t2} = -ig^2\Big(\frac{\alpha}{4\pi}\Big)\bar{v}(p_1)[V^x_{21}\not{\epsilon}_1(\not{q}_1 - \not{p}_1)\not{\epsilon}_2 - V^x_{23}(p_2.\epsilon_2)\not{\epsilon}_1](a_t + b_t\gamma_5)u(p_2), \tag{90}$$

After some manipulation the combined amplitude from the box diagrams in Fig. 7(c) is reduced to

$$\begin{aligned}\mathcal{M}_{b1} + \mathcal{M}_{b2} = &-8ig^2(p_1.q_1)\Big(\frac{\alpha}{4\pi}\Big)[\bar{v}(p_1)\gamma^\mu(a_s + b_s\gamma_5)u(p_2)\Gamma_{\mu\nu\lambda}\epsilon_1^\nu\epsilon_2^\lambda]C_0^{\mathrm{IRD}}(p_1, -q_1, m_e, \lambda, M_W) \\ &-2ig^2\Big(\frac{\alpha}{4\pi}\Big)\bar{v}(p_1)[(p_2.\epsilon_2)\not{\epsilon}_1 - (p_1.\epsilon_1)\not{\epsilon}_2](a_t + b_t\gamma_5)u(p_2)C_0^{\mathrm{IRD}}(p_1, -q_1, m_e, \lambda, M_W).\end{aligned} \tag{91}$$

We note that V^x_{13}, V^x_{23}, V^x_{11}, and V^x_{21} in Eqs. (89) and (90) are given by

$$V^x_{13} = V^x_{23} = 2C_0^{\mathrm{IRD}}(p_1, -q_1, m_e, \lambda, M_W), \tag{92}$$

$$V^x_{11} = V^x_{21} = -4(p_1.q_1)C_0^{\mathrm{IRD}}(p_1, -q_1, m_e, \lambda, M_W). \tag{93}$$

Adding all the contributions from diagrams in Fig 7(c), we have, from Eqs. (89), (90), and (91),

$$\mathcal{M}_{t1} + \mathcal{M}_{t2} + \mathcal{M}_{b1} + \mathcal{M}_{b2} = -8ig^2(p_1.q_1)\Big(\frac{\alpha}{4\pi}\Big)C_0^{\mathrm{IRD}}(p_1, -q_1, m_e, \lambda, M_W)\mathcal{M}^{\mathcal{T}}. \tag{94}$$

Once again we have obtained the factorization of the amplitude. The differential cross section arising from the above amplitude is

$$\frac{d\sigma^{\mathrm{IRIV}}_{t\ \mathrm{channel}}}{d\cos\theta} = -\frac{\alpha}{\pi}(4p_1 \cdot q_1)C_0^{\mathrm{IRD}}(p_1, -q_1, m_e, \lambda, M_W)\frac{d\sigma_0}{d\cos\theta}. \tag{95}$$

Using

$$C_0^{\mathrm{IRD}}(p_1, -q_1, m_e, \lambda, M_W) = \Big(\frac{1}{2p_1.q_1}\Big)\ln\Big(\frac{-t}{\lambda^2}\Big)\ln\Big(\frac{M_W^2 - t}{m_e M_W}\Big), \tag{96}$$

one may write Eq. (95) as

$$\frac{d\sigma^{\mathrm{IRIV}}_{t\ \mathrm{channel}}}{d\cos\theta} = -2\frac{\alpha}{\pi}\frac{d\sigma_0}{d\cos\theta}\ln\Big(\frac{-t}{\lambda^2}\Big)\ln\Big(\frac{M_W^2 - t}{m_e M_W}\Big); \tag{97}$$

TABLE XI. Bremsstrahlung differential cross section in pb for various center-of-mass energies and $a = 0.1$.

θ (deg)	$((\frac{d\sigma}{d\cos\theta})_B(200\text{ GeV}), \delta_B^{\text{total}})$	$((\frac{d\sigma}{d\cos\theta})_B(500\text{ GeV}), \delta_B^{\text{total}})$	$((\frac{d\sigma}{d\cos\theta})_B(1000\text{ GeV}), \delta_B^{\text{total}})$
10	(-34.2446, -0.2201)	(-65.3503, -0.2244)	(-19.5905, -0.2359)
30	(-24.0332, -0.2247)	(-8.1994, -0.2475)	(-2.1896, -0.2734)
50	(-13.8036, -0.2325)	(-2.5477, -0.2683)	(-0.6537, -0.2976)
70	(-8.1109, -0.2419)	(-1.0713, -0.2860)	(-0.2653, -0.3167)
90	(-5.1752, -0.2517)	(-0.5767, -0.3025)	(-0.1405, -0.3339)
110	(-3.5939, -0.2616)	(-0.3718, -0.3189)	(-0.0906, -0.3511)
130	(-2.6759, -0.2709)	(-0.2411, -0.3367)	(-0.0571, -0.3701)
150	(-2.1297, -0.2787)	(-0.1327, -0.3574)	(-0.0270, -0.3943)
170	(-1.8633, -0.2834)	(-0.0634, -0.3805)	(-0.0068, -0.4319)

the corresponding infrared infinite bremsstrahlung contribution is [see Eq. (70)]

$$\frac{d\sigma^{\text{IRIB}}_{t\text{ channel}}}{d\cos\theta} = 2\frac{\alpha}{\pi}\frac{d\sigma_0}{d\cos\theta}\ln\Big(\frac{-t}{\lambda^2}\Big)\ln\Big(\frac{M_W^2 - t}{m_e M_W}\Big). \tag{98}$$

Again the divergences cancel as is explicit from the above two equations.

The only IRIB term which now remains is a u-channel term [see Eq. (71)]. A similar argument to that used for the above t-channel calculation is used to cancel the remaining u-channel IRIB term in Eq. (71). Although we shall not repeat the steps here a few remarks are in order.

(1) The two fermion line crossed box diagrams of Fig. 4(d) replace the triangle diagrams of Fig. 7(c), since there are no u-channel virtual triangle corrections. These precisely generate a contribution similar to the one given in Eqs. (89) and (90).

(2) The crossed box diagrams of Fig. 7(d) take the place of the direct boxes in Fig. 7(c). The expression generated by the diagrams of Fig. 7(d) can be obtained from Eq. (98) by replacing $t \to u$ in Eq. (98) and adding an overall sign change.

Defining

$$C_{01} = C_0^{\text{IR,finite}}(q_2, q_1, M_W, \lambda, M_W), \tag{99}$$

$$C_{02} = C_0^{\text{IR,finite}}(p_1, -q_1, m_e, \lambda, M_W), \tag{100}$$

$$C_{03} = C_0^{\text{IR,finite}}(p_1, -q_2, m_e, \lambda, M_W), \tag{101}$$

the total *finite* contribution is now written as

$$\delta^{\text{total}}_{B,\text{finite}} = \delta^1_{B,\text{finite}} + \delta^2_{B,\text{finite}} + \delta^3_{B,\text{finite}} + \delta^4_{B,\text{finite}} + \delta^5_{B,\text{finite}} + \delta^6_{B,\text{finite}} + \delta^7_{B,\text{finite}}. \tag{102}$$

Here

$$\delta^1_{B,\text{finite}} = -\Big(\frac{\alpha}{\pi}\Big)\Big[\ln(a^2) + \ln(a^2) + \ln\Big(\frac{s}{M_W^2}\Big) + \Big(\frac{1}{\beta_W}\Big)\ln\Big(\frac{1-\beta_W}{1+\beta_W}\Big)\Big], \tag{103}$$

$$\delta^2_{B,\text{finite}} = -\Big(\frac{\alpha}{\pi}\Big)\Big[\Big(\frac{s - 2M_W^2}{s\beta_W}\Big)\ln\Big(\frac{1-\beta_W}{1+\beta_W}\Big)\ln(a^2) - \ln\Big(\frac{s}{m_e^2}\Big)\ln(a^2)\Big], \tag{104}$$

$$\delta^3_{B,\text{finite}} = -\Big(\frac{\alpha}{\pi}\Big)\Big[2\ln\Big(\frac{M_W^2 - u}{M_W^2 - t}\Big)\ln(a^2) + 2\ln\Big(\frac{M_W^2 - u}{M_W m_e}\Big)\ln\Big(\frac{s}{-u}\Big) - 2\ln\Big(\frac{M_W^2 - t}{M_W m_e}\Big)\ln\Big(\frac{s}{-t}\Big)\Big], \tag{105}$$

$$\delta^4_{B,\text{finite}} = -\Big(\frac{\alpha}{\pi}\Big)\Big(-\frac{s - 2M_W^2}{s\beta_W}\Big)\Big[2\text{Sp}\Big(\frac{1-\beta_W}{1+\beta_W}\Big) - \frac{1}{2}\ln^2\Big(\frac{1-\beta_W}{1+\beta_W}\Big) - \frac{\pi^2}{3} + 2\ln\Big(\frac{1-\beta_W}{1+\beta_W}\Big)\ln\Big(\frac{2\beta_W}{1+\beta_W}\Big)\Big], \tag{106}$$

$$\delta^5_{B,\text{finite}} = -\Big(\frac{\alpha}{\pi}\Big)\Big\{2\Big[\text{Sp}\Big(1 - \frac{1}{2}\frac{s(1-\beta_W)}{M_W^2 - t}\Big) + \text{Sp}\Big(1 - \frac{1}{2}\frac{s(1+\beta_W)}{M_W^2 - t}\Big)\Big]\Big\}, \tag{107}$$

$$\delta^6_{B,\text{finite}} = -\Big(\frac{\alpha}{\pi}\Big)\Big\{-2\Big[\text{Sp}\Big(1 - \frac{1}{2}\frac{s(1-\beta_W)}{M_W^2 - u}\Big) + \text{Sp}\Big(1 - \frac{1}{2}\frac{s(1+\beta_W)}{M_W^2 - u}\Big)\Big]\Big\}, \tag{108}$$

$$\delta^7_{B,\text{finite}} = -\Big(\frac{\alpha}{\pi}\Big)[-4(q_1.q_2)C_{01} + 4(p_1.q_1)C_{02} - 4(p_1.q_2)C_{03}]. \tag{109}$$

The finite bremsstrahlung differential cross section is calculated for $a = 0.1$ and $a = 0.05$ and the results are listed in Tables XI and XII respectively. These results are plotted in Figs. 8 and 9. We recall the definition of a from Eq. (72). As is clear from Eq. (109) we have absorbed IR finite parts of the C integrals in the definition of our bremsstrahlung δ, Eq. (102). Although in the above discussion about the cancellations of infrared divergences we have focused or written out only the infinite parts [ones that have $\ln(\lambda)$ terms] it is to be *understood* that finite parts are also included. In particular this means that whenever a C or D integral appears [19,20]

TABLE XII. Bremsstrahlung differential cross section in pb for $a = 0.05$.

θ (deg)	$((\frac{d\sigma}{d\cos\theta})_B(200\text{ GeV}), \delta_B^{\text{total}})$	$((\frac{d\sigma}{d\cos\theta})_B(500\text{ GeV}), \delta_B^{\text{total}})$	$((\frac{d\sigma}{d\cos\theta})_B(1000\text{ GeV}), \delta_B^{\text{total}})$
10	(-45.5995, -0.2930)	(-86.4441, -0.2968)	(-25.8741, -0.3115)
30	(-31.9715, -0.2990)	(-10.8196, -0.3266)	(-2.8831, -0.3600)
50	(-18.3357, -0.3089)	(-3.3536, -0.3531)	(-0.8610, -0.3910)
70	(-10.7547, -0.3207)	(-1.4070, -0.3757)	(-0.3479, -0.4151)
90	(-6.8497, -0.3332)	(-0.7558, -0.3964)	(-0.1839, -0.4369)
110	(-4.7488, -0.3457)	(-0.4864, -0.4172)	(-0.1184, -0.4586)
130	(-3.5308, -0.3575)	(-0.3149, -0.4397)	(-0.0744, -0.4828)
150	(-2.8071, -0.3674)	(-0.1731, -0.4663)	(-0.0352, -0.5137)
170	(-2.4546, -0.3733)	(-0.0826, -0.4960)	(-0.0088, -0.5622)

which has an internal photon line, it is to be understood that the C and D integrals have been decomposed such that the IR divergence is reduced [or written] in terms of C_0 only and some non IR divergent pieces. Hence for the sake of completeness in [19,20] when we give triangle and box virtual corrections we include the complete expressions (containing IR, ultraviolet infinite terms) it should be clear that these have been canceled as indicated. The complete analytic expressions for the C_0 will not be repeated here; it suffices to remark that their analytic computation proceeds in a parallel fashion to the one outlined by 't Hooft and Veltman [25] (see Appendix E of [25], in particular Eqs. E.1–E.3). We obtain expressions identical to the ones given by [15]. Some comments on the bremsstrahlung differential cross section will be included in the next section.

VII. CONCLUSION

As stressed before there are three tests on the correctness of our computations.

(1) The final results must be independent of the mass scale and all ultraviolet pieces must drop out: this indeed turns out to be the case [19], see also Sec. IV.

(2) The final results are independent of the photon mass in the limit of zero photon mass.

(3) The cancellation of the linear and quadratic divergences [11,2] when the SUSY particles are included provides a check on the correctness of our calculation.

Showing the consistency of the adopted renormalization scheme is much more than a formal exercise since it ensures the correctness of the relative signs between the various parts of the radiative corrections. Moreover it acts as a check on the magnitude of the corrections. The box diagrams are ultraviolet finite; however, some of the box diagrams contain infrared infinities (see Sec. VI and Fig. 7). This provides an excellent check on some of the box diagrams since subtle combinations of the box and the triangle diagrams are required (see Section VI) to cancel the bremsstrahlung infinities. Another precaution that we took to check our numerical results was that we computed some of the vertices and self-energy diagrams by hand calculator and compared these to the results obtained by the computer. The numerical calculation was divided into several parts so that errors (if any) did not propagate and that errors could be easily isolated and corrected. Large logarithm terms [such as $\ln^2(m_e^2/s)$] were cancelled by hand so as to avoid numerical instabilities.

The lowest-order differential cross section with respect to the center of mass is very asymmetric (see Fig. 10 and

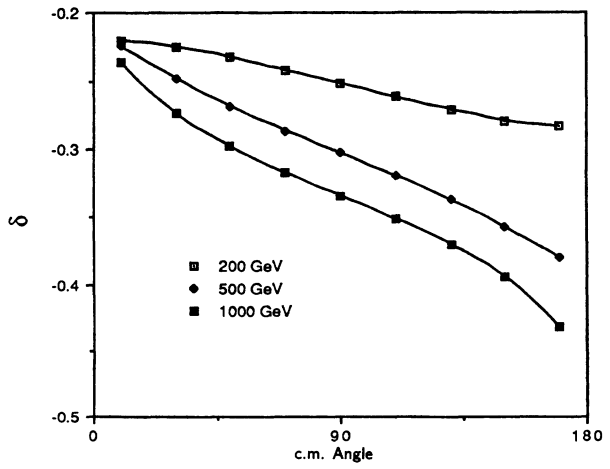

FIG. 8. Angular dependence of the bremsstrahlung corrections relative to the tree level differential cross section with $a = 0.1$.

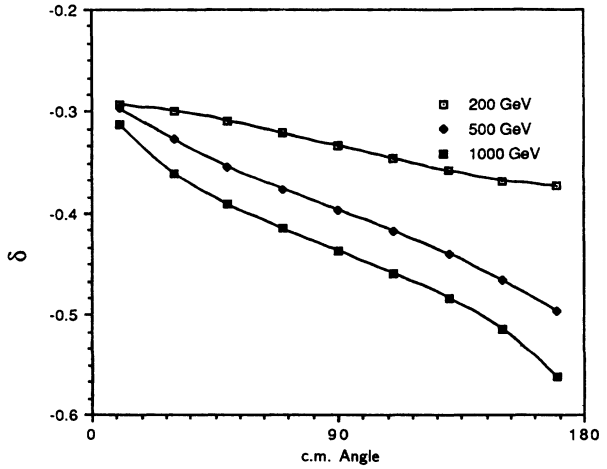

FIG. 9. Angular dependence of the bremsstrahlung corrections relative to the tree level differential cross section with $a = 0.05$.

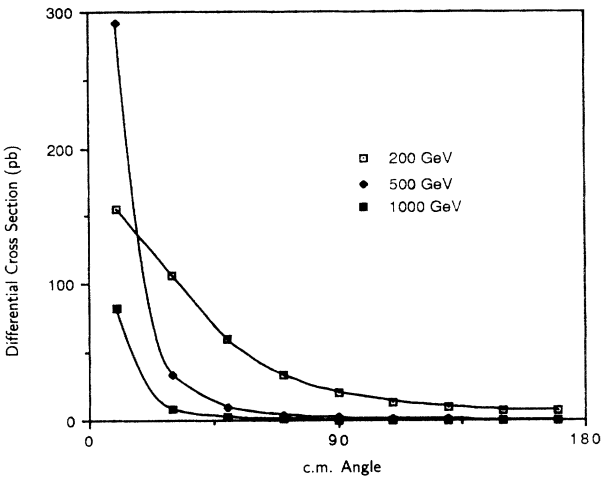

FIG. 10. The tree level differential cross section for three different center-of-mass energies.

Table II). It peaks very strongly near small angles. This peaking gets more pronounced as center-of-mass energy is increased, as can be seen from Fig. 10. This peaking comes entirely from the t-channel neutrino exchange diagram [see Fig. 1(d)].

Next we consider the bremsstrahlung contributions to the one-loop-corrected differential cross section. We have given the complete finite expression for this contribution in Sec. VI [see Eq. (102)]. We note that we have absorbed the IR finite parts of the C integrals [see Eq. (109), also see Eqs. (99)–(101)] in the definition of our bremsstrahlung δ, Eq. (102). This is a matter of choice since the total δ can be written as a sum of the bremsstrahlung δ and the δ from the virtual corrections. The numerical results are listed in Tables XI and XII and plotted in Figs. 10 and 9 respectively. We recall the definition of the parameter a, which is the cutoff parameter and essentially represents a measure of the W energy hidden in the soft photons. We notice from Tables XI and XII and Figs. 10 and 9 that although there is asymmetric peaking at small c.m. angles, it is less pronounced than at the tree level. The reason for this is that the bremsstrahlung differential cross section is related to the tree level differential cross section via δ [see Eq. (66)], which is a nontrivial function of center-of-mass energy and center-of-mass angle. In fact the absolute magnitude of δ increases with increasing the center-of-mass angle and energy (see Tables XI and XII).

In conclusion we have reported the first part of our [11] calculations on the radiative corrections of the process $e^+e^- \longrightarrow W^+W^-$ to one loop in the context of a minimal supersymmetric extension of quantum flavor dynamics. Our tree level results agree with [13,22,15] when one takes into account the slightly different values of the input parameters. After all the one loop radiative corrections are summed [19,20] we find that the QFD part of these corrections are in quite good agreement with Lemoine and Veltman [12] (at the order of 1% of[6] δ) and at the order of $\frac{1}{2}$%–10% of δ with Bohm *et al.* [14].

[6] δ denotes the percentage radiative corrections.

ACKNOWLEDGMENTS

The author would like to thank Professor M.K. Sundaresan and Professor P. Kalyniak for useful discussions and for allowing him to check his QFD result against theirs, and R. Sinha and Professor M.K. Sundaresan for their close assistance in the computer program. The sophisticated parts of the computer program were developed by R. Sinha. Many thanks must go to Gaetan Laberge for his help in making Feynman diagrams with xfig. I would also like to thank the Physics Department at Carleton University for its financial support.

APPENDIX A: SELF-ENERGY OF THE ELECTRON NEUTRINO

As already mentioned in Sec. IV we follow the method of Passarino and Veltman [24] for the evaluation of the Feynman integrals. Since our metric convention is different from theirs, this leads to some trivial sign changes. We have checked our results against theirs and find agreement. For illustration we outline our [11] derivations of the A and B integrals. To this end recall the definitions given in Eqs. (45), and (46) of the A and B integrals:

$$A(m) = -\frac{1}{i\pi^2}\int d^n q \frac{1}{[q^2 - m^2]}, \tag{A1}$$

$$B_0; B_\mu; B_{\mu\nu} = \frac{1}{i\pi^2}\int d^n q \frac{1; q_\mu; q_\mu q_\nu}{[q^2 - m_1^2][(q+k)^2 - m_2^2]}. \tag{A2}$$

We now consider the explicit derivation of the A integral. Using the definition A1 and formulas for the n-dimensional loop integrals [26] [Table B4 of [26], page 478] one obtains, after a little algebra,

$$A(m) = m^2\Big[-\triangle - 1 + \ln\Big(\frac{m^2}{M_W^2}\Big)\Big]. \tag{A3}$$

Next we must evaluate B_0, B_1 , B_{21}, and B_{22} where these arise in the definitions Eq. (A2). The function B_μ must be proportional to k_μ; this defines B_1. Similarly B_{21} and B_{22} are defined or extracted from $B_{\mu\nu}$:

$$B_\mu = B_1 k_\mu,$$
$$B_{\mu\nu} = B_{21} k_\mu k_\nu - B_{22} g_{\mu\nu}.$$

Using the above definitions, Feynman-parametric technique and dimensional regularization B_0 through B_{22} are evaluated [24,11] with the results

$$B_0 = \triangle - \int_0^1 dx \ln\Big(\frac{M^2}{M_W^2}\Big), \tag{A4}$$

$$M^2 = x m_2^2 + (1-x) m_1^2 - x(1-x) k^2, \tag{A5}$$

$$B_1 = -(1/2)\,\triangle + \int_0^1 x dx \ln\Big(\frac{M^2}{M_W^2}\Big), \tag{A6}$$

$$B_{21} = (1/3)\,\triangle - \int_0^1 x^2 dx \ln\Big(\frac{M^2}{M_W^2}\Big), \tag{A7}$$

$$B_{22} = -(1/4)(\triangle + 1)[m_1^2 + m_2^2 - (1/3)k^2] + (1/2)\int_0^1 dx M^2 \ln\Big(\frac{M^2}{M_W^2}\Big). \tag{A8}$$

Alternatively [24,11] one knows that the functions B_1, B_{21}, and B_{22} are algebraically related to A and B_0. One may find these relations by using the definitions for the A and B integrals. Once these relations are found, and having explicit forms for the A and B_0 on hand, one may use these algebraic relations to express B_1, B_{21}, and B_{22} in terms of A and B_0:

$$p^2 B_1 = (1/2)[-A(m_1) + A(m_2) + (m_2^2 - m_1^2 - k^2)B_0], \tag{A9}$$

$$p^2 B_{21} - B_{22} = (1/2)[-A(m_2) + (m_2^2 - m_1^2 - k^2)B_1], \tag{A10}$$

$$p^2 B_{21} - 4B_{22} = m_1^2 B_0 - A(m_2) + (1/2)[m_1^2 + m_2^2 - (1/3)k^2]. \tag{A11}$$

Expressions (A10) and (A11) can be solved to obtain B_{21} and B_{22} in terms of A and B_0.

Next we turn to the neutrino self-energy. There are three diagrams, Fig. 3, contributing to the neutrino self-energy in QFD. It is straightforward to write out the contributions of these. Defining $\nu_i(k^2)\not{k}\frac{(1-\gamma_5)}{2}$ to be the self-energy due to the ith particle one has [Fig. 3(a)]

$$\nu_W(k^2) \doteq \frac{(2-n)}{2}[B_0(M_W, m_e, k^2) + B_1]. \tag{A12}$$

Similarly for diagrams 2 and 3 one obtains Fig. 3:

$$\nu_{G^+}(k^2) \doteq -(m_e^2/2M_W^2)[B_0(m_{H^+}, m_e, k^2) + B_1] \tag{A13}$$

and

$$\nu_Z(k^2) \doteq \frac{(2-n)}{2}(1/2c_W^2)[B_0(M_Z, m_{\nu_e}, k^2) + B_1]. \tag{A14}$$

These results agree with Sakakibara [23], thus providing a check on our calculations. Replacing each particle in the self-energy loops of Fig. 3 by its s partners one obtains the SUSY contribution to neutrino self-energy (Fig. 3, 1′, 2′, 2′a, and 3′). These are written respectively as

$$\nu_{\tilde{w}}(k^2) \doteq [B_1(m_{\tilde{\omega}}, m_{\tilde{e}}, k^2)], \tag{A15}$$

$$\nu_{H^+}(k^2) \doteq -(m_e^2/2M_W^2)[B_0(m_{H^+}, m_{\tilde{e}}, k^2) + B_1], \tag{A16}$$

$$\nu_{\tilde{w}}(k^2) \doteq (m_e^2/M_W^2)[B_1(m_{\tilde{\omega}}, m_{\tilde{e}}, k^2)], \tag{A17}$$

$$\nu_{\tilde{z}}(k^2) \doteq (1/2c_W^2)[B_1(m_{\tilde{z}}, m_{\tilde{\nu_e}}, k^2)]. \tag{A18}$$

We follow the notation that in each set of square brackets all the B's have the same argument as the first B in the brackets. We note that there are two contributions due to the W-ino; one to the order (m_e^2/M_W^2). This arises because the W-ino in our model [2,11] is made of two parts, one being the fermionic partner of the charged Higgs scalar (H^+) and the other being of course the s partner of the W boson.

Now a few remarks are in order, as it is well known in SUSY theories that superficial linear divergences and quadratic divergences cancel [2,11] among boson and fermion degrees of freedom. We [11] have shown that the cancellation of the quadratic and superficial linear divergences indeed occurs in our specific model. The strategy we have used to show these cancellations closely parallels that of Haber and Kane [2] (see Appendix E, Pt. 7 of [2]). We first write down the contributions arising to self-energy from all the particles and then from the very outset we group together the contributions to a particular particle from a physical multiplet (physical multiplets are given in Sec. I). It is then easily seen how the divergences cancel within each group. An explicit example of our method is outlined for the case of the W self-energy in Appendix E.

For the case of the neutrino we can follow the above method, or, simply, if we compare the contributions to the neutrino self-energy given in Eqs. (A12)–(A18), we see that all the superficially linearly divergent terms cancel. We note that from the definition of B_1 it is superficially linearly divergent hence we must check that all the B_1 contributions cancel. It follows immediately from Eqs. (A12)–(A18) that all the B_1 contributions cancel.

APPENDIX B: SELF-ENERGY OF THE ELECTRON

The calculation of the self-energy diagrams for the electron is much like the neutrino case except that there are a few additional diagrams Fig. 4. Defining

$$L = \frac{(1-\gamma_5)}{2},\ R = \frac{(1+\gamma_5)}{2},$$
$$a_1 = (1/4)(2 - 4s_W^2),\ b_1 = (1/4)(-4s_W^2) \tag{B1}$$

the contributions for the diagrams of Fig. 4 may be promptly written as (we recall that $\doteq$ is equivalent to $= \frac{g^2}{16\pi^2}$)

$$\Sigma_\gamma \doteq s_W^2[(2-n)\{B_0(\lambda, m_e, k^2) + B_1\}\not{k} + n m_e B_0](L+R), \tag{B2}$$

where a mass λ has been given to the photon:

$$\Sigma_W \doteq \frac{(2-n)}{2}[B_0(M_W, m_{\nu_e}, k^2) + B_1]\not{k}L, \quad \text{(B3)}$$

$$\Sigma_Z \doteq \frac{1}{c_W^2}[(2-n)\{B_0(M_Z, m_e, k^2) + B_1\}\not{k}(a_1^2 L + b_1^2 R) + n m_e a_1 b_1 B_0(L+R)], \quad \text{(B4)}$$

$$\Sigma_{G^+} \doteq -(m_e^2/2M_W^2)[B_0(M_W, m_{\nu_e}, k^2) + B_1]\not{k}R, \quad \text{(B5)}$$

$$\Sigma_{H_1^0} \doteq -(m_e^2/4M_W^2)[\{B_0(m_{H_1^0}, m_e, k^2) + B_1\}\not{k} + m_e B_0](L+R), \quad \text{(B6)}$$

$$\Sigma_{G^0} \doteq -(m_e^2/4M_W^2)[\{B_0(m_{G^0}, m_e, k^2) + B_1\}\not{k} - m_e B_0](L+R), \quad \text{(B7)}$$

$$\Sigma_{\tilde{\gamma}} \doteq 2s_W^2[B_1(m_{\tilde{\gamma}}, m_{\tilde{e}}, k^2)]\not{k}L,$$
$$\Sigma_{\tilde{\gamma}} \doteq 2s_W^2[B_1(m_{\tilde{\gamma}}, m_{\tilde{e}}, k^2)]\not{k}R, \quad \text{(B8)}$$

$$\Sigma_{\tilde{\omega}} \doteq [B_1(m_{\tilde{\omega}}, m_{\tilde{\nu_e}}, k^2)]\not{k}L,$$
$$\Sigma_{\tilde{\omega}} \doteq \frac{m_e^2}{M_W^2}[B_1(m_{\tilde{\omega}}, m_{\tilde{\nu_e}}, k^2)]\not{k}R, \quad \text{(B9)}$$

$$\Sigma_{H^+} \doteq -\frac{m_e^2}{2M_W^2}[B_0(m_{H^+}, m_{\tilde{\nu_e}}, k^2) + B_1]\not{k}R, \quad \text{(B10)}$$

$$\Sigma_{\tilde{z}} \doteq \frac{2a_1^2}{c_W^2}[B_1(m_{\tilde{z}}, m_{\tilde{e}}, k^2)]\not{k}L,$$
$$\Sigma_{\tilde{z}} \doteq \frac{2b_1^2}{c_W^2}[B_1(m_{\tilde{z}}, m_{\tilde{e}}, k^2)]\not{k}R,$$
$$\Sigma_{\tilde{z}} \doteq \frac{m_e^2}{2M_W^2}[B_1(m_{\tilde{z}}, m_{\tilde{e}}, k^2)]\not{k}L,$$
$$\Sigma_{\tilde{z}} \doteq \frac{m_e^2}{2M_W^2}[B_1(m_{\tilde{z}}, m_{\tilde{e}}, k^2)]\not{k}R, \quad \text{(B11)}$$

$$\Sigma_{H_2^0} \doteq -(m_e^2/4M_W^2)[\{B_0(m_{H_2^0}, m_e, k^2) + B_1\}\not{k} + m_e B_0](L+R), \quad \text{(B12)}$$

$$\Sigma_{\tilde{h}} \doteq \frac{m_e^2}{2M_W^2}[B_1(m_{\tilde{h}}, m_{\tilde{e}}, k^2)]\not{k}L,$$
$$\Sigma_{\tilde{h}} \doteq \frac{m_e^2}{2M_W^2}[B_1(m_{\tilde{h}}, m_{\tilde{e}}, k^2)]\not{k}R, \quad \text{(B13)}$$

$$\Sigma_{H_3^0} \doteq -(m_e^2/4M_W^2)[\{B_0(m_{H_3^0}, m_e, k^2) + B_1\}\not{k} - m_e B_0](L+R). \quad \text{(B14)}$$

From the photon contribution to the electron self-energy we extract the infrared infinite parts

$$f_L \doteq -s_W^2\left[2\ln\left(\frac{\lambda^2}{m_e^2}\right)\right],$$
$$\delta Z_R \doteq -s_W^2\left[2\ln\left(\frac{\lambda^2}{m_e^2}\right)\right]. \quad \text{(B15)}$$

We [11] have shown that all the superficial linear divergences in the electron self-energy contributions cancel in our supersymmetric model.

APPENDIX C: SELF-ENERGY OF THE PHOTON

In this and the three subsequent sections we concern ourself with computation of self-energies of gauge mesons. Some simple remarks are in order. First of all, as is clear from Fig. 11, the γ self-energy can be categorized into two sets, one entirely due to fermions and the other arising out of γ interaction with W-boson (G denotes the Goldstone boson mode associated with W and $c^{\pm}$ are the Faddeev-Popov ghosts corresponding to each of the W^+ and W^-). One immediately writes down π (where π has been defined in Sec. IV) arising from fermions:

$$\pi_f^{\gamma}(k^2) \doteq -\sum_{f,c} n s_W^2 Q_f^2[(n-2)B_{22}(m_f, m_f, k^2) - B_{21}k^2 - B_1 k^2 + m_f^2 B_0]. \quad \text{(C1)}$$

The gauge-boson contribution may be written down as

$$\pi_{\mathrm{GB}}^{\gamma}(k^2) \doteq s_W^2[B_0(M_W, M_W, k^2) - 12B_1 - 12B_{21} + \tfrac{2}{3}]. \quad \text{(C2)}$$

Equations (C1) and (C2) allow us to write the renormalized $\tilde{\pi}$:

$$\tilde{\pi}_{f+\mathrm{GB}}^{\gamma}(k^2) \doteq \pi_{f+\mathrm{GB}}^{\gamma}(k^2) - \pi_{f+\mathrm{GB}}^{\gamma}(0). \quad \text{(C3)}$$

Here,

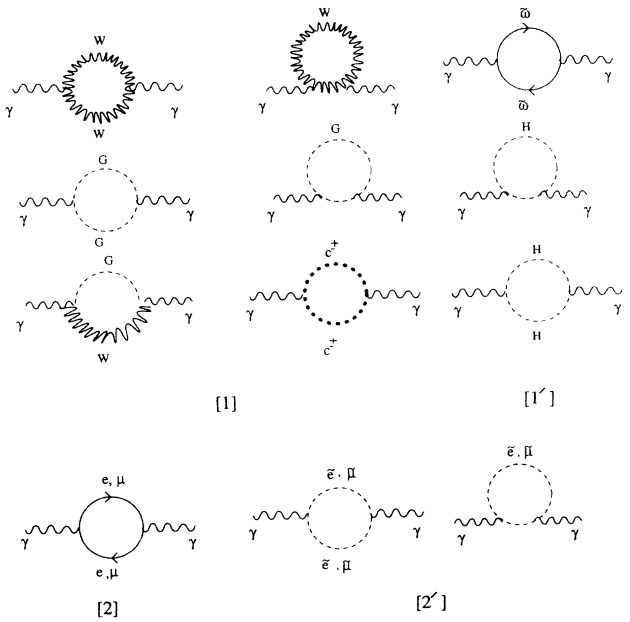

FIG. 11. One loop Feynman diagrams contributing to the photon self-energy in SQFD.

$$\pi^{\gamma}_{f+g.b}(0) \doteq s^2_W\Big[3\,\triangle + \frac{2}{3} + \frac{4}{3}Q^2_f \sum_{f,c}\Big\{-\triangle + \ln\Big(\frac{m^2_f}{M^2_W}\Big) + \frac{1}{2}\Big\}\Big]. \quad \text{(C4)}$$

The SUSY contribution to the photon self energy is displayed in Fig. 11, 1′ and 2′. The contribution of the W-ino works out to be

$$\pi^{\gamma}_{\tilde{\omega}}(k^2) \doteq -2ns^2_W[(n-2)B_{22}(m_{\tilde{\omega}}, m_{\tilde{\omega}}, k^2) - B_{21}k^2 - B_1k^2 + m^2_{\tilde{\omega}}B_0] \quad \text{(C5)}$$

The charged Higgs boson (H^+) gives

$$\pi^{\gamma}_{H^+}(k^2) \doteq s^2_W[-4B_{22}(m_{H^+}, m_{H^+}, k^2) + 2A(m_{H^+})]. \quad \text{(C6)}$$

The calculation for Fig. 11, 2′ follows a similar pattern to the charged Higgs scalar, since it is also a vector-scalar-scalar interaction and in a renormalizable theory it has a universal form, summing over all colors and flavors:

$$\pi^{\gamma}_{\tilde{f}}(k^2) \doteq \sum_{f,c} 2s^2_W Q^2_f[-4B_{22}(m_{\tilde{f}}, m_{\tilde{f}}, k^2) + 2A(m_{\tilde{f}})]. \quad \text{(C7)}$$

We have checked that quadratic, superficial quadratic, and superficial linear divergences cancel as expected in SUSY for the case of photon self-energy.

APPENDIX D: $\gamma - Z$ MIXING

We do not display the diagrams which contribute to γ-Z mixing since they are identical to those of the photon diagrams. The fermion contribution in QFD is

$$a^{\gamma-Z}_f(k^2) \doteq -\sum_{f,c} nt_W Q_f\Big(\frac{1}{2}T_{3f} - Q_f s^2_W\Big)[(n-2)B_{22}(m_f, m_f, k^2) - B_{21}k^2 - B_1k^2 + m^2_f B_0]. \quad \text{(D1)}$$

The gauge-boson contribution may be written down as

$$a^{\gamma-Z}_{\rm GB}(k^2)t_W[c^2_W k^2[B_0(M_W, M_W, k^2) - 12B_1 - 12B_{21} + \frac{2}{3}] + \frac{1}{2}k^2[B_0(M_W, M_W, k^2) + 4B_1 + 4B_{21}] + 2M^2_W B_0]. \quad \text{(D2)}$$

The SUSY contributions to $\gamma - Z$ are now given. The contribution of the W-ino works out to be

$$\pi^{\gamma-Z}_{\tilde{\omega}}(k^2) \doteq -n(c^2_W + a_1)t_W[(n-2)B_{22}(m_{\tilde{\omega}}, m_{\tilde{\omega}}, k^2) - k^2(B_{21} + B_1) + m^2_{\tilde{\omega}}B_0]. \quad \text{(D3)}$$

The charged Higgs boson (H^+) gives

$$a^{\gamma-Z}_{H^+}(k^2) \doteq \frac{1}{2}t_W(1 - 2s^2_W)[-4B_{22}(m_{H^+}, m_{H^+}, k^2) + 2A(m_{H^+})]. \quad \text{(D4)}$$

Finally the sfermion contribution to the γ-Z reads

$$a^{\gamma-Z}_{\tilde{f}}(k^2) \doteq \sum_{i,f,c} t_W\Big(\frac{1}{2}T^i_{3f} - Q^i_f s^2_W\Big)Q^i_f[-4B_{22}(m_{\tilde{f}}, m_{\tilde{f}}, k^2) + 2A(m_{\tilde{f}})]. \quad \text{(D5)}$$

We have checked that quadratic and superficial divergences (linear and quadratic) cancel as expected in SUSY for the case of photon-Z mixing diagrams.

APPENDIX E: W SELF-ENERGY

The W-self energy diagrams can be divided into four categories: the contribution from fermions, from Higgs bosons, from the photon, and finally from the Z boson (Fig. 12). The contribution from the fermions may be written as

$$a^W_f \doteq \sum_{\text{doublets},c}\Big[\frac{n}{4}[(2-n)B_{22}(m_1, m_2, k^2) + k^2(B_1 + B_{21})]\Big]. \quad \text{(E1)}$$

The contribution from the Higgs particle reads

$$a^W_{H^0_1} \doteq \frac{1}{4}[-4B_{22}(m_{H^0_1}, M_W, k^2) - 4M^2_W B_0 + A(m_{H^0_1})]. \quad \text{(E2)}$$

The contribution from the gauge boson (GB) sector to the W self-energy may be written as

$$a^W_{\rm GB} \doteq s^2_W(-\frac{k^2}{3}+M^2_W)+c^2_W(\frac{2k^2}{3}-2M^2_W+2M^2_Z)-\frac{1}{2}M^2_W+\frac{1}{4}M^2_Z+(\frac{M^2_Z}{4}$$
$$+3M^2_W)\ln\frac{M^2_W}{M^2_Z}-s^2_W[5k^2\{-B_0(\lambda,M_W,k^2)-2B_1-2B_{21}\}+M^2_W(B_0$$
$$+8B_1)]+c^2_W[k^2\{-3B_0(M_Z,M_W,k^2)-20B_1-12B_{21}\}-6(M^2_W$$
$$-M^2_Z)(-B_0-B_1)]+(\frac{1}{4}-c^2_W)[k^2\{-2B_0(M_Z,M_W,k^2)-6B_1-4B_{21}\}$$
$$-2(M^2_W-M^2_Z)(-B_0-B_1)]+(c^2_W+2-\sec^2\theta_W)M^2_W B_0(M_Z,M_W,k^2). \quad \text{(E3)}$$

We note that we have checked our results against Sakakibara [23] for the contributions from the standard particles and found agreement. Now the contribution from the sparticles can be written, from the Higgsino,

$$a^W_{\tilde h} \doteq \frac{n}{4}[(2-n)B_{22}(m_{\tilde h},m_{\tilde\omega},k^2)+k^2(B_1+B_{21})], \quad \text{(E4)}$$

from the photino,

$$a^W_{\tilde\gamma} \doteq n s^2_W[(2-n)B_{22}(m_{\tilde\gamma},m_{\tilde\omega},k^2)+k^2(B_1+B_{21})], \quad \text{(E5)}$$

from the Z-ino,

$$a^W_{\tilde z} \doteq n\Big(c^2_W+\frac{1}{4}\Big)[(2-n)B_{22}(m_{\tilde z},m_{\tilde\omega},k^2)+k^2(B_1+B_{21})]-nm_{\tilde\omega}m_{\tilde z}c_W B_0, \quad \text{(E6)}$$

from H^0_2,

$$a^W_{H^0_2} \doteq \frac{1}{4}[-4B_{22}(m_{H^0_2},m_{H^+},k^2)+A(m_{H^0_2})+A(m_{H^+})], \quad \text{(E7)}$$

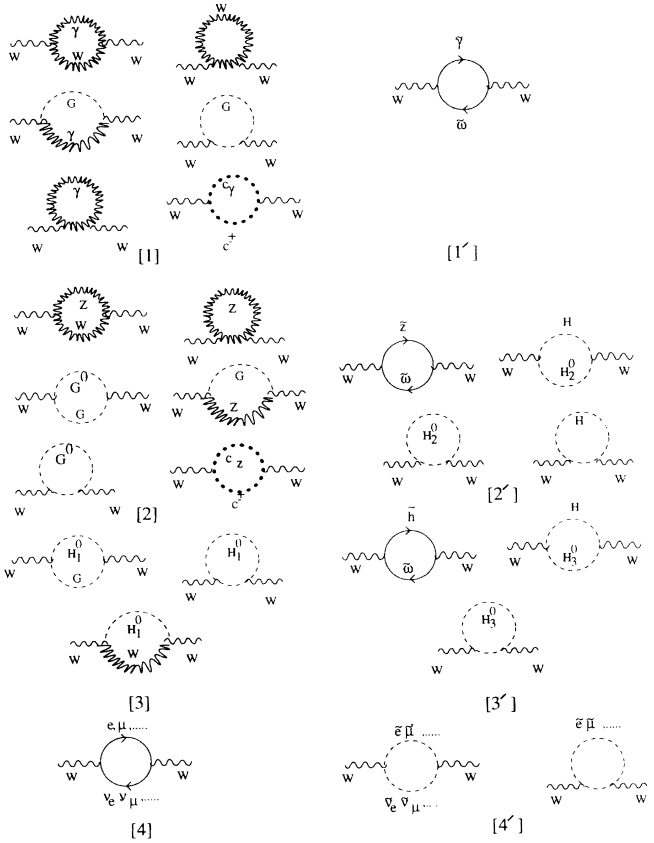

FIG. 12. One loop Feynman diagrams contributing to the W-boson self-energy in SQFD.

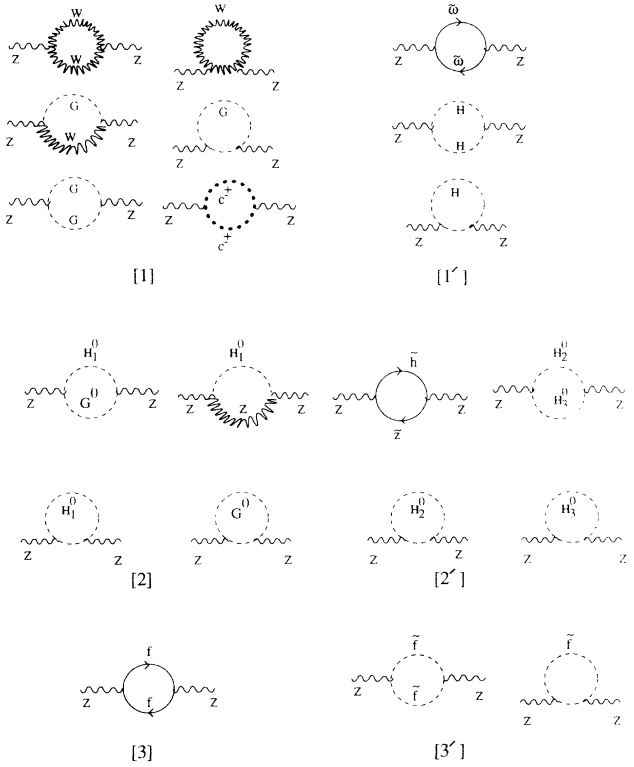

FIG. 13. One loop Feynman diagrams contributing to the Z-boson self-energy in SQFD.

from H_3^0,

$$a^W_{H_3^0} \doteq \frac{1}{4}[-4B_{22}(m_{H_3^0}, m_{H^+}, k^2) + A(m_{H_3^0}) + A(m_{H^+})], \tag{E8}$$

and, finally from scalar fermions,

$$a^W_{\tilde{f}} \doteq \sum_{\text{doublets,c}} \Big[\frac{1}{2}[-4B_{22}(m_1, m_2, k^2) + A(m_1) + A(m_2)]\Big]. \tag{E9}$$

We note that m_1 and m_2 being respectively the masses of the down and the up sfermions.

The derivative of the renormalized a^W [Eq. (28)] which enters as the relevant quantity is easily extracted from the above evaluations of the various a's and the definition of δZ_W [see Eq. (30)]:

$$\frac{\partial \tilde{a}^W(s)}{\partial s}_{s=M_W^2} = \frac{\partial a^W(s)}{\partial s}_{s=M_W^2} - \delta Z_W. \tag{E10}$$

From the photon contribution to the W self-energy we extract the infrared infinite part

$$\frac{\partial \tilde{a}^W(s)}{\partial s}_{s=M_W^2} \doteq -s_W^2\Big[2\ln\Big(\frac{\lambda^2}{M_W^2}\Big)\Big]. \tag{E11}$$

To illustrate the cancellation of quadratic and linear divergences in our SUSY $\mathrm{SU}(2)_L \times \mathrm{U}(1)_Y$ model in the gauge-boson sector consider the W self-energy. As is clear from Fig. 12 we have suitably divided the various contributions to the W self-energy to make such cancellations apparent; for example, we would expect the fermion contribution (diagram 4 in Fig. 12) to receive such cancellations from the sfermions (diagram 4′ in Fig. 12). Considering only one doublet of fermions for simplicity we have (taking the SUSY limit, i.e., $m_{\tilde{f}} = m_f$)

$$T_{\mu\nu,\,f} + T_{\mu\nu,\,s-f} = g^2 \int \frac{d^n q}{(2\pi)^n} \frac{N_{\mu\nu}}{[q^2 - m_1^2][(q+k)^2 - m_2^2]}. \tag{E12}$$

Here

$$N_{\mu\nu}(2 - \frac{n}{2})q_\mu q_\nu + (1 - \frac{n}{4})(q_\mu k_\nu + k_\mu q_\nu) + \frac{1}{2}k_\mu k_\nu + [(\frac{n}{4} - 1)q^2 + (\frac{n}{4} - 1)k\cdot q + \frac{1}{2}(m_1^2 + m_2^2 - k^2)]g_{\mu\nu} \tag{E13}$$

Note that in (E12) m_1 and m_2 are the mass of the up and down fermion (sfermion). Setting $n = 4 + \varepsilon$, it is clear that the quadratic and linearly divergent terms are rendered harmless. Using the definitions of B's in Appendix A and definition of $a^W(k^2)$ after some algebra, one gets

$$a^W_{f+sf}\varepsilon(-\frac{1}{2}B_{22} + \frac{k^2}{4}B_{21} + \frac{k^2}{4}B_1) + \frac{1}{2}(m_1^2 + m_2^2 - k^2)B_0 \tag{E14}$$

Hence the only divergence left is an logarithmic one which is enshrined in B_0. The Higgs-Higgsino sector gives (see Diagrams 3 and 3′ in Fig. 12), in the SUSY limit $m_{\tilde{h}} = m_{H_3^0} = m_{H_1^0}$, $m_{\tilde{\omega}} = m_{H^+} = M_W$,

$$T_{\mu\nu,\,\tilde{h}} + T_{\mu\nu,\,H_1^0} + T_{\mu\nu,\,H_3^0} + T_{\mu\nu,\,H^+} g^2 \int \frac{d^n q}{(2\pi)^n} \frac{N_{\mu\nu}}{[q^2 - m^2_{H_1^0}][(q+k)^2 - M_W^2]}. \tag{E15}$$

Here

$$N_{\mu\nu}(2 - \frac{n}{2})q_\mu q_\nu + (1 - \frac{n}{4})(q_\mu k_\nu + k_\mu q_\nu) + \frac{1}{2}k_\mu k_\nu + [(\frac{n}{4} - 1)q^2 + (\frac{n}{4} - 1)k\cdot q + \frac{1}{2}(m^2_{H_1^0} + M_W^2 - k^2) - M_W^2]g_{\mu\nu}. \tag{E16}$$

Setting $n = 4 + \varepsilon$ in (E16) it is clear again that quadratic and linear divergences cancel. Finally $a_{\text{Higgs-Higgsino}}$, extracted from (E16), reads

$$a^W_{\text{Higgs+Higgsino}} \doteq \varepsilon(-\tfrac{1}{2}B_{22} + \tfrac{k^2}{4}B_{21} + \tfrac{k^2}{4}B_1) + \tfrac{1}{2}(m^2_{H_1^0} + M_W^2 - k^2)B_0 - M_W^2 B_0. \tag{E17}$$

Similar results were found in the $(\gamma, \tilde{\gamma})$ and $(Z, H_2^0, \tilde{z})$ sectors and will not be repeated here.

APPENDIX F: Z SELF-ENERGY

The contributions to the Z self-energy are given in Fig. 13. The contribution to the Z self-energy from the standard particles is found to be, from the fermions,

$$a_f^Z \doteq -\sum_{f,c} \frac{n}{c_W^2}\{[(g_V^f)^2+(g_A^f)^2][(n-2)B_{22}(m_1,m_2,k^2)-k^2(B_1+B_{21})]+[(g_V^f)^2-(g_A^f)^2]m_f^2 B_0\}, \tag{F1}$$

where $g_V^f = \frac{1}{2}(T_3^f)_L - s_W^2 Q_f$ and $g_A^f = -\frac{1}{2}(T_3^f)_L$, see [4], from the Higgs bosons,

$$a_{H_1^0}^Z \doteq \frac{1}{4c_W^2}[-4B_{22}(m_{H_1^0},M_Z,k^2)-4M_Z^2 B_0 + A(m_{H_1^0})], \tag{F2}$$

and, from the gauge bosons (GB's),

$$\begin{aligned} a_{\rm GB}^Z \doteq{}& \frac{2k^2c_W^2}{3} - \frac{M_Z^2}{4c_W^2}\left(1+\ln\frac{M_W^2}{M_Z^2}\right) - c_W^2 k^2[-B_0(M_W,M_W,k^2)+12B_1+12B_{21}] \\ &+\left(\frac{1}{4c_W^2}-1\right)k^2[-B_0(M_W,M_W,k^2)-4B_1-4B_{21}] \\ &+\left(4-\frac{2}{c_W^2}\right)M_W^2 B_0(M_W,M_W,k^2). \end{aligned} \tag{F3}$$

The contribution from the sparticles reads

$$a_{\tilde h}^Z \doteq \frac{n}{4c_W^2}[(2-n)B_{22}(m_{\tilde h},m_{\tilde z},k^2)+k^2(B_1+B_{21})], \tag{F4}$$

$$a_{\tilde\omega}^Z \doteq n\left(c_W^2+\frac{(1-2s_W^2)^2}{4c_W^2}\right)[(2-n)B_{22}(m_{\tilde\omega},m_{\tilde\omega},k^2)+k^2(B_1+B_{21})] - n(1-2s_W^2)m_{\tilde\omega}m_{\tilde\omega}B_0, \tag{F5}$$

$$a_{H_2^0,H_3^0}^Z \doteq \frac{1}{4c_W^2}[-4B_{22}(m_{H_3^0},m_{H_2^0},k^2)+A(m_{H_2^0})+A(m_{H_3^0})], \tag{F6}$$

$$a_{H^+}^Z \doteq \frac{(1-2s_W^2)^2}{4c_W^2}[-4B_{22}(m_{H^+},m_{H^+},k^2)+2A(m_{H^+})], \tag{F7}$$

$$a_{\tilde f}^Z \doteq \sum_{i,f,c}\frac{2}{c_W^2}\{[(g_V^f)^2+(g_A^f)^2][-4B_{22}(m_{\tilde f},m_{\tilde f},k^2)+2A(m_{\tilde f})]\}. \tag{F8}$$

$m_{\tilde f}$ is the mass of the sfermion.

We have checked that quadratic and superficial divergences (linear and quadratic) cancel as expected in SUSY for the case of Z self-energy diagrams.

[1] *Physics at LEP I*, Proceedings of the Workshop, Geneva, Switzerland, 1989, edited by G. Altarelli, R. Kleiss, and C. Verzegnassi (CERN Report No. 89-08, Geneva, 1989), Vols. 1 and 3.

[2] H.E. Haber and G.L. Kane, Phys. Rep. **117**, 75 (1985); see also J.F. Gunion, H.E. Haber, G. Kane, and S. Dawson, *The Higgs Hunter's Guide* (Addison-Wesley, Reading, MA, 1990).

[3] *Proceedings of the ECFA Workshop on LEP 200*, Aachen, West Germany, 1986, edited by A. Bohm and W. Hoogland (CERN Report No. 87-08, Geneva, Switzerland, 1987).

[4] V. Barger and R. Phillips, *Collider Physics* (Addison-Wesley, Reading, MA, 1987).

[5] J. Baily *et al.*, Nucl. Phys. **B150**, 1 (1979).

[6] R. Bates, J.N. Ng, and P. Kalyniak, Phys. Rev. D **34**, 172 (1986); P. Kalyniak, R. Bates, and J. Ng, *ibid.* **33**, 755 (1986).

[7] S. Alam, Phys. Rev. D **39**, 2801 (1989), and references therein.

[8] J.A. Grifols *et al.*, Nucl. Phys. **B253**, 4756 (1985).

[9] K. Schwarzer, Oxford University Report No. 40/84, 1984 (unpublished).

[10] B.W. Lynn, Report No. SLAC-PUB-3358, 1984 (unpublished).

[11] S. Alam, Ph.D. thesis, Ottawa-Carleton Institute for Physics, 1992; P. Kalyniak and M.K. Sundaresan, Int. J. of Mod. Phy. A **3**, 2101 (1988); S. Alam, J. Sci. Technol. (to be published).

[12] M. Lemoine and M. Veltman, Nucl. Phys. **B164**, 445 (1980).

[13] R. Philippe, Phys. Rev. D **26**, 1588 (1982).

[14] M. Bohm *et al.*, Nucl. Phys. **B304**, 463 (1988).

[15] J. Fleischer *et al.*, Z. Phys. C **42**, 409 (1989).

[16] Particle Data Group, J.J. Hernández *et al.*, Phys. Lett. B **239**, 1 (1990).

[17] J.D. Bjorken and S.D. Drell, *Relativistic Quantum Mechanics* (McGraw-Hill, New York, 1964).

[18] B. De Wit and D. Z. Freedman, Phys. Rev. D **12**, 2286 (1975).

[19] S. Alam, following paper, Phys. Rev. D **50**, 148 (1994).
[20] S. Alam, this issue, Phys. Rev. D **50**, 174 (1994).
[21] H. Baer, M. Drees, and X. Tata, Phys. Rev. D **41**, 3414 (1990).
[22] W. Alles *et al.*, Nucl. Phys. **B119**, 125 (1977).
[23] S. Sakakibara, Phys. Rev. D **24**, 1149 (1981); also in *Workshop on Radiative Corrections in* $SU(2)_L \times U(1)_Y$, Proceedings of the Workshop, Trieste, Italy, 1993, edited by B.W. Lynn and J.F. Wheater (World Scientific, Singapore, 1994).
[24] G. Passarino and M. Veltman, Nucl. Phys. **B160**, 151 (1979).
[25] G. 't Hooft and M. Veltman, Nucl. Phys. **B153**, 365 (1979).
[26] G. Ross, *Grand Unified Theories* (Benjamin/Cummings, New York, 1985).